

Eline Nyhus

Flux-smelting behavior and aluminothermic reduction of a pre- reduced Mn ore

Master's thesis in Materials Science and Engineering

Supervisor: Jafar Safarian

June 2023

Eline Nyhus

Flux-smelting behavior and aluminothermic reduction of a pre- reduced Mn ore

Master's thesis in Materials Science and Engineering
Supervisor: Jafar Safarian
June 2023

Norwegian University of Science and Technology
Faculty of Natural Sciences
Department of Materials Science and Engineering



Preface

This report describes the Flux-smelting behavior and aluminothermic reduction of a pre-reduced Mn ore and is part of the Horizon Europe project HAlMan. It is the author's master thesis and serves as the main evaluation basis for the course TMT4900 at the Norwegian University of Science and Technology, NTNU, and the work was performed at the Department of Materials Science and Engineering.

First, I would like to thank my supervisor at NTNU, Professor Jafar Safarian, for all his support throughout the project and for giving me the opportunity of writing my specialization project and master thesis for the HAlMan project.

I hereby declare that the work in this thesis has been performed independently and in accordance with the examination regulations at the Norwegian University of Science and Technology (NTNU).

Trondheim, June 2023

Eline Nyhus

Abstract

This master's thesis presents an experimental study conducted to explore the smelting and aluminothermic smelting-reduction processes of a pre-reduced Mn ore using lime and Al metal. The aim of the study is to investigate the flux-smelting behavior and aluminothermic reduction of a pre-reduced Mn ore and the flux-smelting behavior of MnO and CaO by differential scanning calorimetry (DSC), microstructure analysis and phase analysis.

Smelting of the pre-reduced and lime occurred at 1500°C with a CaO/Al₂O₃ molar ratio of 1. At a molar ratio of 0.8, only sintering occurred.

The results show that aluminothermic reduction occurred for all the samples in the 1300-1500°C, although the extent of reaction was lower at 1300°C. Processing time of 0.5h, 1h, and 1.5h was investigated for the samples at 1500°C. It was found that the processing time did not affect the metal yield to a large extent. Notably, the produced slags contained a leachable mayenite (C12A7) phase, which is a significant Al₂O₃-containing compound suitable for potential alumina recovery from the slags.

Table of Contents

Preface	i
Abstract	iii
1. Introduction	1
1.1 Background.....	1
1.2 Aim of project.....	2
2. Theory	3
2.1 Manganese.....	3
2.1.1 Mineralogy.....	3
2.1.2 Application of manganese.....	4
2.1.3 Production of ferromanganese alloys.....	5
2.2 Thermodynamics.....	7
2.2.1 Reduction of Mn oxides.....	7
Pre-reduction by CO gas.....	7
Pre-reduction by H ₂	8
Reduction by C.....	10
Reduction by Al.....	11
2.3 Literature review on aluminothermic reduction of MnO.....	11
2.4 Mn-Fe system.....	13
2.5 Calcium-aluminat phase diagram.....	15
2.6 CaO-Al ₂ O ₃ -MnO.....	16
2.7 Differential scanning calorimetry.....	18
3. Methodology	20
3.1 Experimental procedure.....	20
3.2 Materials.....	22

3.3	<i>Sample preparation</i>	24
3.4	<i>Furnace operation</i>	26
3.5	<i>Microstructural analysis</i>	28
3.6	<i>Phase analysis</i>	28
3.7	<i>Differential scanning calorimetry</i>	29
4.	Results	31
4.1	<i>Flux-smelting behavior of the pre-reduced ore</i>	31
4.1.1	Differential scanning calorimetry	31
4.1.2	Microstructure of flux-smelted pre-reduced ore.....	32
4.1.3	Phase analysis of the smelted pre-reduced ore.....	34
4.1.4	Mass loss and visual observations	37
4.2	<i>Aluminothermic smelting-reduction of pre-reduced ore</i>	40
4.2.1	Microstructural analysis	40
4.2.2	Produced metals compositions	50
4.2.3	Slag composition and phases.....	51
4.2.4	Phase analysis of produced slags.....	52
4.2.5	Mass loss and visual observations	53
5.	Discussion	55
5.1	<i>Effect of temperature on the flux-smelting on pre-reduced ore</i>	55
5.2	<i>Metal yield and mass loss in aluminothermic reduction trials</i>	56
5.3	<i>Effect of the temperature on aluminothermic reduction</i>	57
5.4	<i>Effect of processing time</i>	58
5.5	<i>Characteristics of the produced slags</i>	59
6.	Conclusions	61

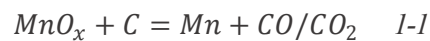
7. Further work.....	62
Bibliografi.....	i
Appendix	v
<i>Appendix 1</i>	<i>v</i>
<i>Appendix 2</i>	<i>viii</i>
<i>Appendix 3</i>	<i>ix</i>

1. Introduction

This chapter introduces today's commercial process for manganese (Mn) through carbothermic reduction, as well as the suggested HALMan process. Lastly, the goals for this project and the assumptions and limitations will be discussed.

1.1 Background

The current technology for Mn-metal production is the carbothermic reduction of Mn ores, shown in an overall process reaction in equation $MnO_x + C = Mn + CO/CO_2$ 1-1 in submerged arc furnaces (SAF) and blast furnaces (BF), where SAF technology is the dominant one.



For SAF, metallurgical coke is the primary energy source and a reduction agent in the process, and the coke consumption is estimated at 300-500 kg per ton of alloy produced. The process is also energy-intensive, using 2000–3000 kWh per ton of metal produced [1] [2].

The HalMan process is based on the idea that Mn_3O_2 , Mn_2O_3 , and MnO_2 can be reduced to MnO by hydrogen as a reducing agent and that further reduction to metallic Mn can be completed by aluminothermic reduction [3]. The process is shown in Figure 1.1-2 where the ore is pre-reduced by H_2 gas in a pre-reduction reactor before smelting reduction furnace (SRF) where Al reduces MnO.

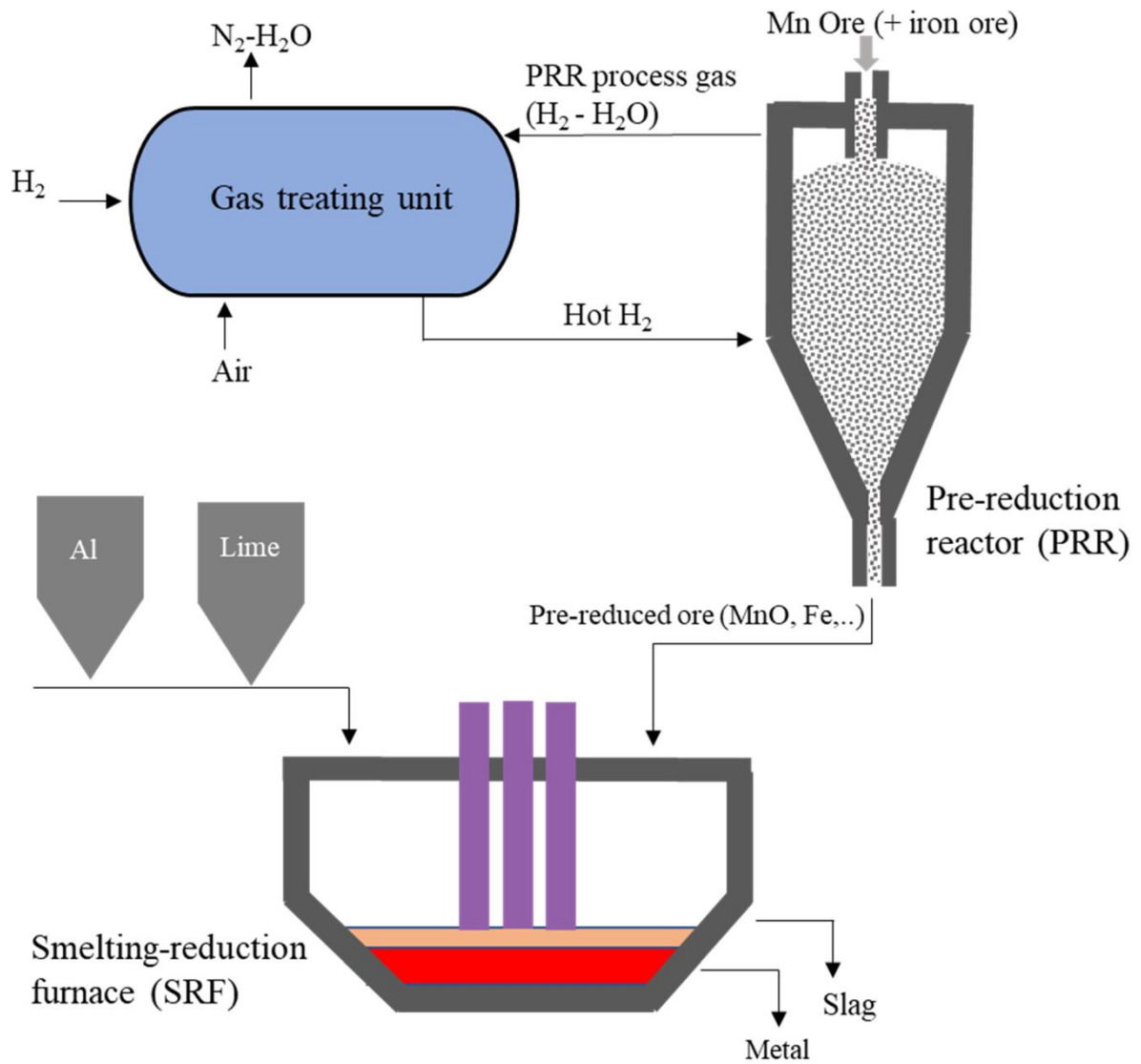


Figure 1-1: Schematic of the proposed HalMan process [3].

1.2 Aim of project

The aim of this project is to:

- investigate the flux-smelting behavior and aluminothermic reduction of a pre-reduced Mn ore.
- Study the flux-smelting behavior of MnO and CaO by differential scanning calorimetry (DSC), microstructure analysis and phase analysis.
- Investigate the microstructure and phases for the metals and slag products and outline the process yield.

2. Theory

2.1 Manganese

Manganese, Mn, is the 12th most abundant element in the earth's crust, and the 4th most used metal behind iron, aluminum, and copper. Mn is a transition metal with an atomic mass of 54.94, a melting point of 1246°C and it is placed in between chromium, Cr, and iron, Fe, in the periodic system. As a pure metal, Mn is considered a silvery, hard, and brittle metal. The demand for Mn is directly linked to the steel industry, with 90% of produced Mn [1].

The EU relies on 93% of Mn ores to be imported from other non-EU countries, with South Africa being the largest supplier. In 2023 the EU defined Mn as a critical raw material and a strategic raw material due to supply risk for the steelmaking industry and battery industry. Here, a strategic raw material is considered important for technologies that support the green and digital transition as well as defense objectives. [4]

2.1.1 Mineralogy

Manganese ores can be classified into three categories based on Mn content. Metallurgical Mn ores, containing more than 35% Mn, are suitable for high or low-grade ferromanganese manufacture. Ferruginous manganese is ores containing 15% - 35% Mn and high levels of iron. Manganiferrous ores with 5% - 10% Mn are usually classified as iron ores and are commonly used to manufacture mangan-ferrous pig iron [5] [1]. Manganese oxide in the form of MnO appears as green crystals and powders [6]

The world's largest land-based manganese ore reserve is in the Republic of South Africa, located in the Kalahari field. Here, two different mineralogies are found, known as Mamatwan and Wessels. Where the Mamatwan ore mainly consists of carbonates, the Wessels ore mainly contains oxides such as Braunite I ($\text{Mn}^{2+}\text{Mn}^{3+}_6(\text{SiO}_4)\text{O}_8$), Braunite II ($\text{CaMn}^{3+}_{14}(\text{SiO}_4)\text{O}_{20}$), Hausmannite ($\text{Mn}^{2+}\text{Mn}^{3+}_2\text{O}_4$), Bixbyite ($(\text{Mn}, \text{Fe})_2\text{O}_3$), and Hematite (Fe_2O_3) [7]. The characteristics of the South-African ores are high basicity and low O/Mn and Mn/Fe ratios. The phosphorous, P, levels are also considered low.

Major Mn-ore-producing countries with high-grade ores are South Africa, Australia, Brazil, and Gabon. China, India, Ukraine, Kazakhstan, and Georgia have mines containing lower-grade

ores. Fig 2-1 shows production estimates for Mn-ore in 2022, presented as thousands of tons of Mn-units produced in the respective countries and regions [8].

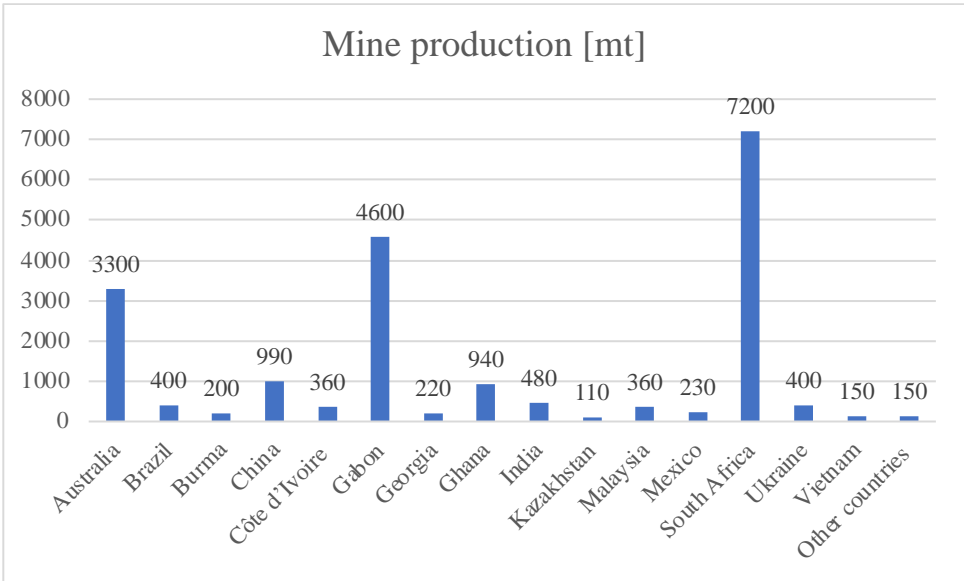


Figure 2-1: The mine production of Mn-ores in 2022 [8].

2.1.2 Application of manganese

As mentioned, around 90% of the Mn produced is related to the steel industry. Given the extensive range of steel types manufactured, the specific manganese-alloy requirements vary depending on the intended product. FeMn and SiMn can be produced with diverse carbon © compositions, including high carbon (HC), medium carbon (MC), low carbon (LC), and ultralow carbon (ULC). Specifications for the alloys are shown in Table 2-1.

Table 2-1: shows the composition of the most common Mn-alloys [1].

Grade	Mn [wt%]	C [wt%]	Si [wt%]	P [wt%]	S [wt%]	B [ppm]
HC FeMn	78	7.5	0.30	0.20	-	-
MC FeMn	80-83	1.0-1.5	0.6	0.20	-	-
LC FeMn	80-83	0.5	0.6	0.20	-	-
SiMn	67-68	1.5-2.0	17-20	0.10-0.15	0.02	200
LC SiMn	59-63	1.5-2.0	25-30	0.10	0.01	100
ULC SiMn	58-62	0.05	27-31	0.05	0.01	100

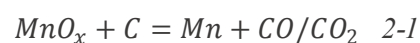
When added as an alloying element, Mn can increase properties like strength, ductility, and hardness. Approximately 70 % of all Mn added to steel serves as an alloying element increasing strength, toughness and hardness¹. If special low-carbon steels are produced, refined FeMn and SiMn can be utilized, thus avoiding additional decarburizing. The remaining 30 % is added as a deoxidizer and for sulfur, S, removal [1].

During the desulfurization of steel utilizing Mn, manganese sulfide, MnS, is formed instead of iron sulfide, FeS. Unlike FeS, MnS does not wet the grain boundaries and has a higher melting point, thereby avoiding metal cracking due to hot shortness [1].

When producing stainless steels, ~1% Mn is normally added, although Mn can completely replace the Ni content, bringing the Mn concentration up to a maximum of ~16 %¹. Mn will also improve the corrosion resistance of Al and strengthen bronzes. Finally, the element can be utilized in non-metallurgical applications such as the oxidizer and disinfectant potassium permanganate, $KMnO_4$, in chemistry and medicine, respectively, or as MnO_2 in dry cell batteries [1].

2.1.3 Production of ferromanganese alloys

The current state of the art technology for Mn-metal production is the carbothermic reduction of Mn ore, shown in equation 2-1, in submerged arc furnaces (SAF) and blast furnaces (BF), where SAF technology is the dominant one.



For SAF, metallurgical coke is the primary energy source and a reduction agent in the process, and the coke consumption is estimated at 2 tons per ton of alloy produced. The process is also energy-intensive, using 2000–3000 kWh per ton of metal produced. Commonly used slags are limestone and dolomite, which contributes to chemical compositions giving viscosity and smelting temperature promoting higher Mn yield. [1] [2]. Figure 2-2 shows a simplified model of the SAF.

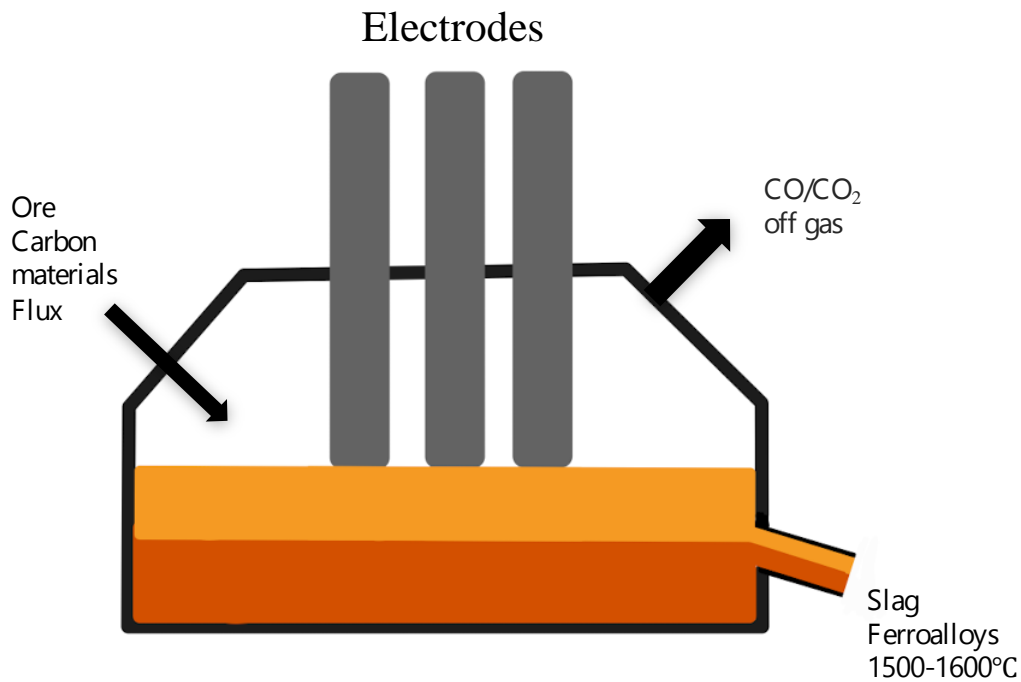


Figure 2-2: Simplified principal sketch of the carbothermic reduction of Mn-ores in a submerged arc furnace (SAF).

The SAF consists of three different zones: the pre-reduction zone, the coke bed zone, and the metal layer. The charge enters the furnace through the pre-reduction zone at 25°C where higher manganese oxides are reduced to lower manganese oxides. Higher manganese oxides are defined as higher manganese oxides with more oxygen than manganese present and include MnO_2 , Mn_2O_3 , and Mn_3O_4 . The reduction of higher manganese oxides to lower is exothermic and contributes heat to the furnace and further process. In the coke bed zone, the temperature is increased, and fluxes and oxides are melting. The lower manganese oxides will be reduced to metallic manganese that descends to the bottom of the furnace. The liquified oxides and fluxes create a liquid slag, floating on top of the metal [1].

2.2 Thermodynamics

2.2.1 Reduction of Mn oxides

Pre-reduction by CO gas

In a CO gas atmosphere, the reduction of higher manganese oxides are exothermic reactions, where energy is released. However, when the Boudouard reaction is initiated at elevated temperatures above 800°C ($\text{CO}_2 + \text{C} = 2\text{CO}$), the total reduction in SAF becomes endothermic due to the reversed Boudouard reaction, as seen in Figure 2-3.

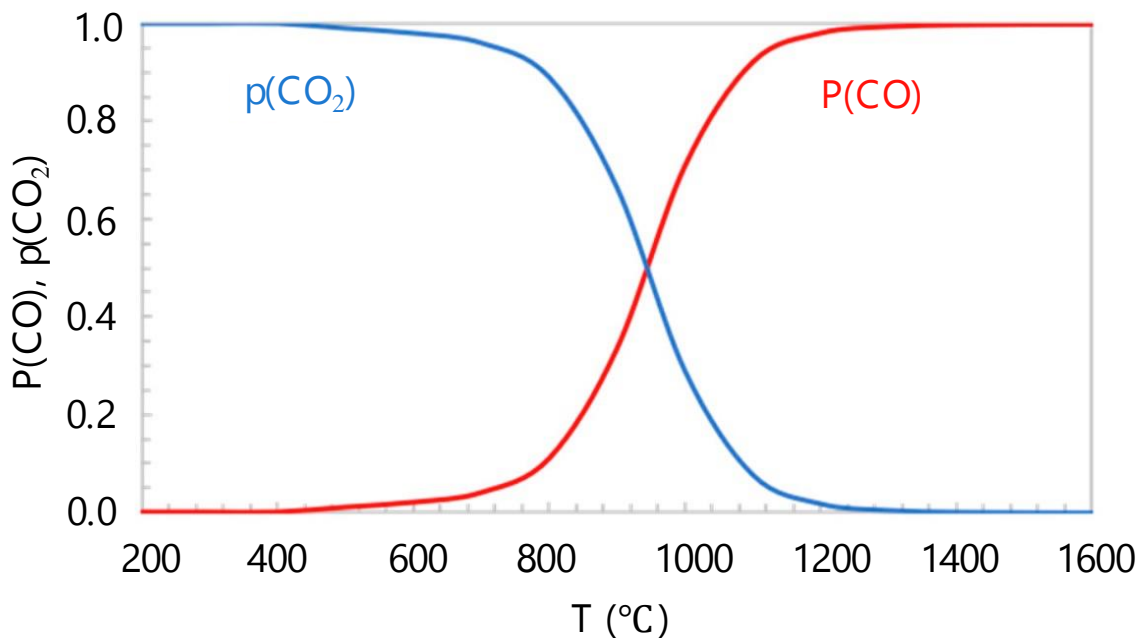


Figure 2-3: Equilibrium diagram for Boudouard reaction with excessive solid carbon available.

Calculations were done by HSC Chemistry.

The reductions of higher manganese oxides in the pre-reduction zone by CO are the following:



Pre-reduction by H₂ gas

The comprehensive investigation of MnO₂ reduction by H₂ gas was initially conducted by Barner. The study revealed that synthetic pyrolusite, when subjected to H₂ gas at temperatures ranging from 200 to 500°C, undergoes a sequential reduction process from MnO₂ to Mn₂O₃, then to Mn₃O₄, and ultimately to MnO [13]. The reduction equations 2-5 to 2-7 depict the stepwise reduction process and the corresponding enthalpy changes ($\Delta H_{25^\circ\text{C}}$), as derived from the HSC database. Equation 2-8 illustrates the overall reduction of Fe₂O₃ by H₂, along with the enthalpy changes (ΔH_{25}) for the reaction. Notably, the reduction of manganese ores to MnO through hydrogen exhibits a higher exothermic nature compared to the reduction of hematite to iron. The reduction of Mn₂O₃ to MnO is accompanied by an enthalpy change of -168.3 kJ/mol, while it is -98.8 kJ/mol for the reduction of Fe₂O₃ to Fe.



In Figure 2-4, the phase stability diagram of MnO₂ in the presence of H₂/H₂O gas is presented. The diagram indicates that MnO is the stable phase within a broad temperature range and at gas mixture fraction of XH₂ = 0.01-0.99, corresponding to a significantly reduced partial pressure of oxygen. The diagram also suggests that complete reduction to Mn(l) is theoretically achievable; however, it is important to note that this would require H₂ gas of at least 99.999% purity. Consequently, it is concluded that practical reduction beyond MnO is not feasible [9].

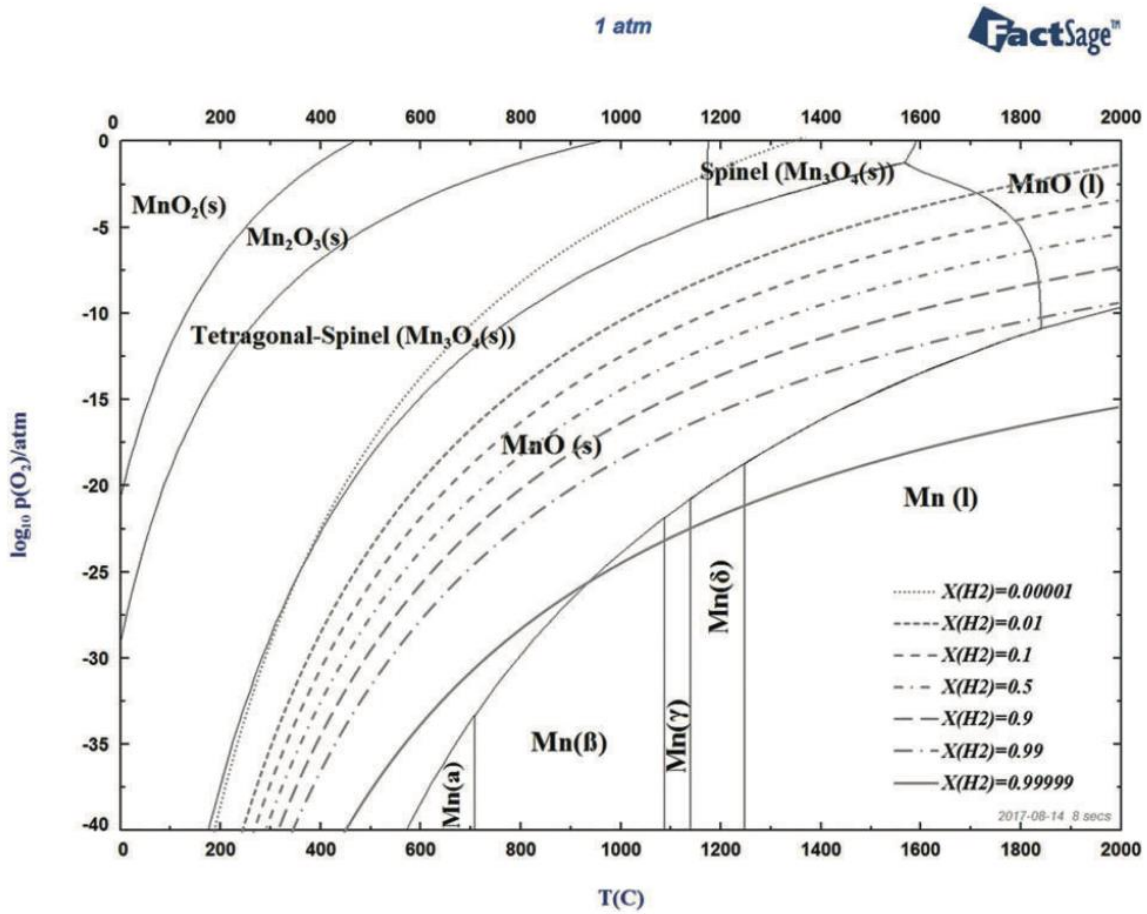


Figure 2-4: predominant phase stability diagram for MnO_2 in the presence of H_2/H_2O [9]

From the semester project of mine in the course TMT4500, it was found that pre-reduction by H_2 yields metallic iron and MnO from Mn_2O_3 and Fe_2O_3 in the ore at temperatures over $500^\circ C$ [10]. Mn ore with 4-10mm particle size was pre-reduced in a thermogravimetric furnace by H_2 -gas. The samples were heated in Ar -gas to set-point and then exposed to H_2 -gas for a given time at the given temperature. The pre-reduction of the Mn ore reached a stationary point at $700^\circ C$ - $1000^\circ C$ as seen in Figure 2-5 below, and the reduction was considered completed at these temperatures. The excess mass loss at $900^\circ C$ - $1000^\circ C$ was considered a loss of volatiles.

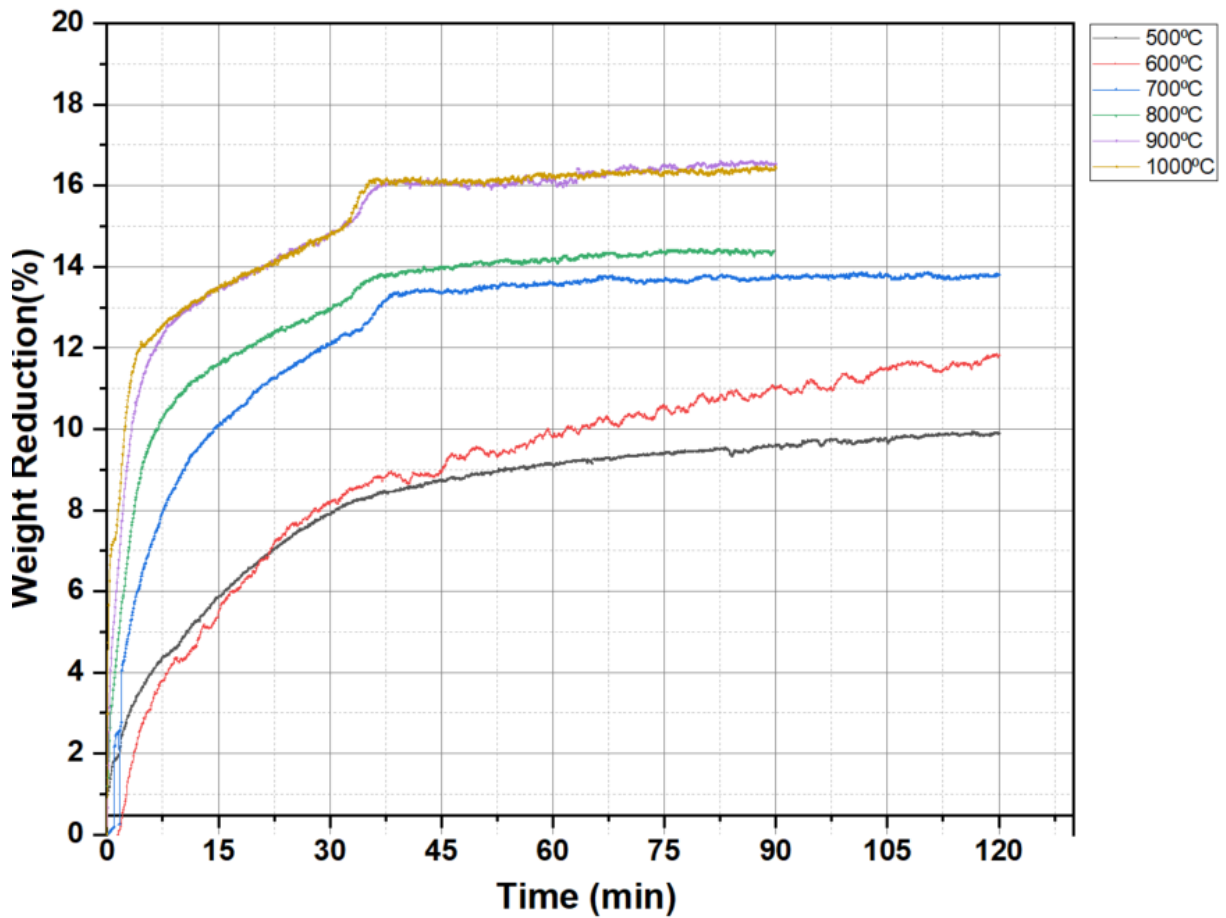


Figure 2-5: Reduction curves in wt% for Mn-ore in H₂ gas from 500°C-1000°C [10].

Reduction by C

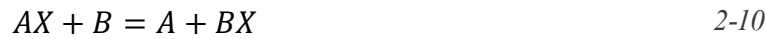
The final reduction step from MnO to Mn mainly takes place in the coke bed zone in a SAF, where C is the reducing agent as seen in equation 2-9:



The ΔH value from HSC Chemistry showing an endothermic reduction reaction. The carbon in the above chemical reaction is the solid carbon, or the dissolved carbon in the molten metal.

Reduction by Al

In the metallothermic reduction, an oxide can be reduced by metal following general equation 2-10:



Where X is the oxygen, fluorine, or chlorine in the oxide, and A and B represent the metals. Equation 2-11 shows the reduction of MnO by Al in HalMan process and the ΔH value from HSC Chemistry showing an exothermic reaction.



2.3 Literature review on aluminothermic reduction of MnO

A review of the existing literature identified a few works on the aluminothermic reduction of MnO by dissolved Al in a continuous galvanizing bath. Some recent studies were found analyzing the results of the aluminothermic reduction of manganese oxides using real industrial materials such as Al dross or FeMn slag.

In the following studies pure Al powders were utilized, and either pure MnO₂ or manganese ore was employed as the source of manganese oxide [[11] [12] [13] [14]] . Dávila et al. [11] investigated the influence of magnesium concentration in molten aluminum, derived from beverage cans, on the aluminothermic reduction process of Mn₂O₃ particles obtained from discharged alkaline battery cathodes. The authors demonstrated the crucial role of magnesium content in the base alloy for aluminothermic reduction. Magnesium enhances the wettability of aluminum on Mn₂O₃ particles, facilitating solid-liquid reactions.

Kavitha and McDermid [12] examined the aluminothermic reduction of MnO using dissolved Al in the continuous galvanizing process. They concluded that the reduction of MnO is a relatively simple dissolution reaction, wherein the composition of the MnO layer remains unchanged throughout the reaction. Additionally, the thickness of the resulting thin Al₂O₃ reaction product remained relatively constant (3-4 nm) for the different reaction times investigated. Jiaying et al. [13] studied the aluminothermic reduction of pure MnO₂ using

metallic Al particles through a thermite process. They investigated the conversion of MnO_2 to Mn_2O_3 and Mn_3O_4 using Differential Scanning Calorimetry (DSC) techniques. They have provided information about heat generation due to the reactions at temperatures below $900\text{ }^\circ\text{C}$, but their experiments did not produce metallic manganese.

Sarangi et al. [14] conducted a study on the reaction between MnO_2 and Al powders using the Differential Thermal Analysis (DTA) technique. They determined the heat generation resulting from aluminothermic reduction reactions, varying the MnO_2/Al ratio. Based on the rate of heat generation observed in DTA experiments, they calculated the reduction reaction rate and performed a kinetic study. Bhoi et al. [15] investigated the aluminothermic reduction of manganese ore particles by Al powder to produce ferromanganese, incorporating lime and fluorspar in their mixtures. They conducted reduction reactions through roasting at moderate temperatures of $650\text{ }^\circ\text{C}$ and $950\text{ }^\circ\text{C}$, resulting in ferromanganese samples with Mn content ranging from 70% to 80% and Fe content ranging from 12% to 16%.

Kudyba et al. [16] investigated the Aluminothermic Reduction of Manganese Oxide from Selected MnO-Containing Slags. The study investigated the aluminothermic reduction process of MnO from different slags using Al. Two types of industrial Al dross and pure Al were tested. The results showed that MnO was completely reduced through the aluminothermic process. The process also led to the reduction of SiO_2 in the industrial ferromanganese slag. A small amount of Ca and Mg migrated into the metal phase, depending on the slag's chemical composition. The study demonstrated the feasibility of using Al dross and ferromanganese slag together to produce Mn, Mn-Al, and Mn-Al-Si alloys. The process had low energy consumption due to highly exothermic reactions at high temperatures. Overall, it was considered that the process offered flexibility and controllable composition of the produced slag.

In another study by Kudyba et al. [17] the Mn and Al recovery from ferromanganese slag and Al white dross by a high-temperature smelting-reduction process was studied. In this study, the recovery of Mn and Al from industrial waste generated during ferromanganese and aluminum production processes was investigated using a high-temperature smelting-aluminothermic reduction process. The experiments involved varying the addition of calcium oxide (CaO) flux and the quality of dross. It was observed that the prepared mixtures of materials resulted in homogeneous metal and slag products with consistent chemical composition and phase distribution. However, the separation of the metal phase from the slag at elevated temperatures

was more pronounced when a higher amount of CaO was added. Viscosity calculations and equilibrium studies revealed that optimal separation of metal and slag occurred when the produced slag had lower viscosity and a lower liquidus temperature. The process successfully yielded Al-Mn-Si alloys while achieving complete recovery of Mn, Si, Fe, and unreacted Al. The quality of the metal product was found to be less dependent on slight variations in the dross quality. However, an increase in the concentration of minor Ca in the metal was observed with a significant increase in CaO content in the slag phase. The viscosity of the produced slag containing Al₂O₃ is significantly influenced by the amount of CaO, decreasing as the CaO content increases. It was found that with more than 30 wt% CaO in the slag, the viscosity could be optimized to below 2 Poise. The liquidus temperature of the slag phase depends significantly on the amount of CaO flux added. Adjusting the added CaO between 40-60% above 1500°C allows for the achievement of a fully molten slag phase. The separation of the molten metal from the coexisting slag phase is enhanced when the slag has a [11] lower viscosity and a lower liquidus temperature.

2.4 Mn-Fe system

Studying the binary Mn-Fe phase diagram is important as the aluminothermic reduction of the pre-reduced Mn ore may yield Mn-Fe alloys. Figure 2-6 shows the equilibrium phase diagram for Mn-Fe calculated from FactStage. The liquid phase is completely miscible, and the liquidus curve reaches a minimum of 1234°C at 12.7% Fe.

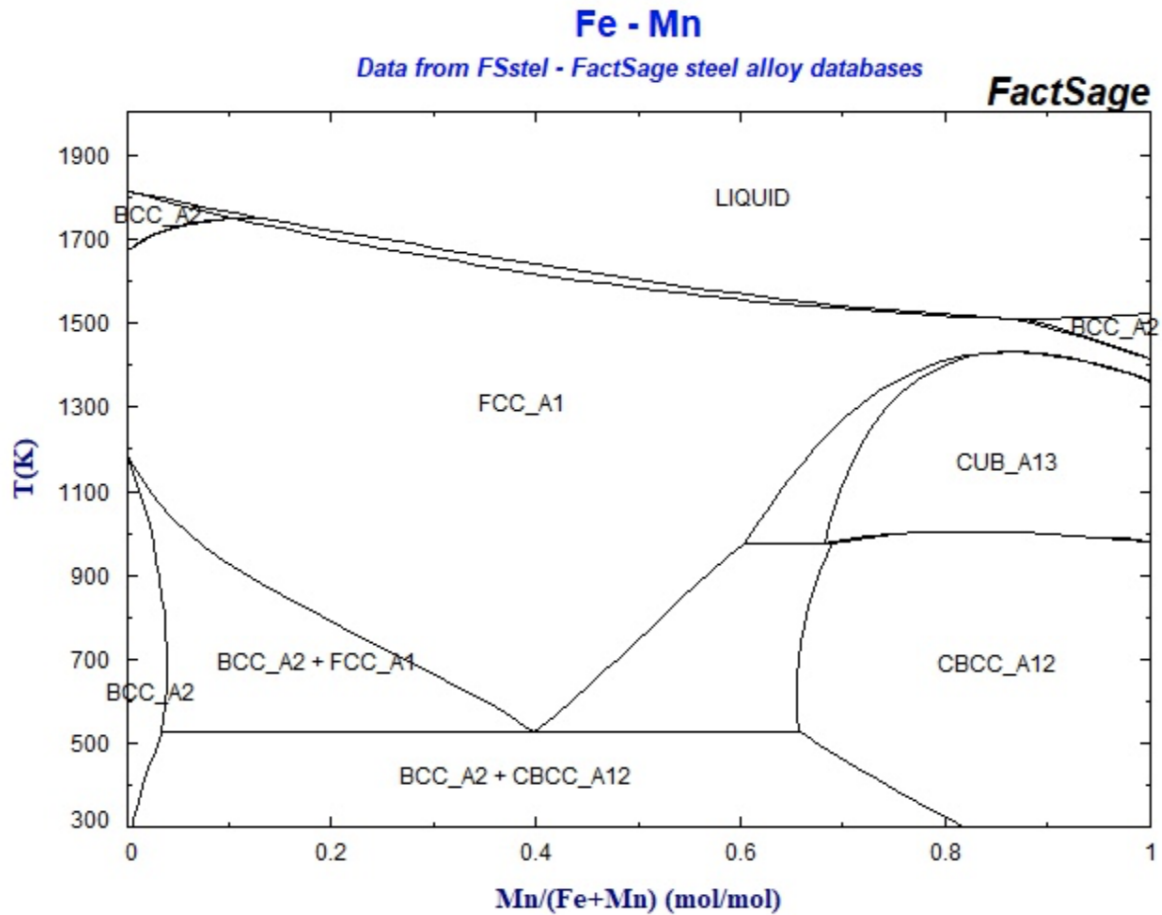


Figure 2-6: The figure shows the binary Fe-Mn system. The data is obtained from the software FactStage.

Figure 2-6 indicates that in a wide composition range the Mn-Fe alloys are molten at temperatures below 1500 C. The chemical activities for the Mn-Fe system are shown in Figure 2-7, and shows the system has very small deviations from ideal behavior.

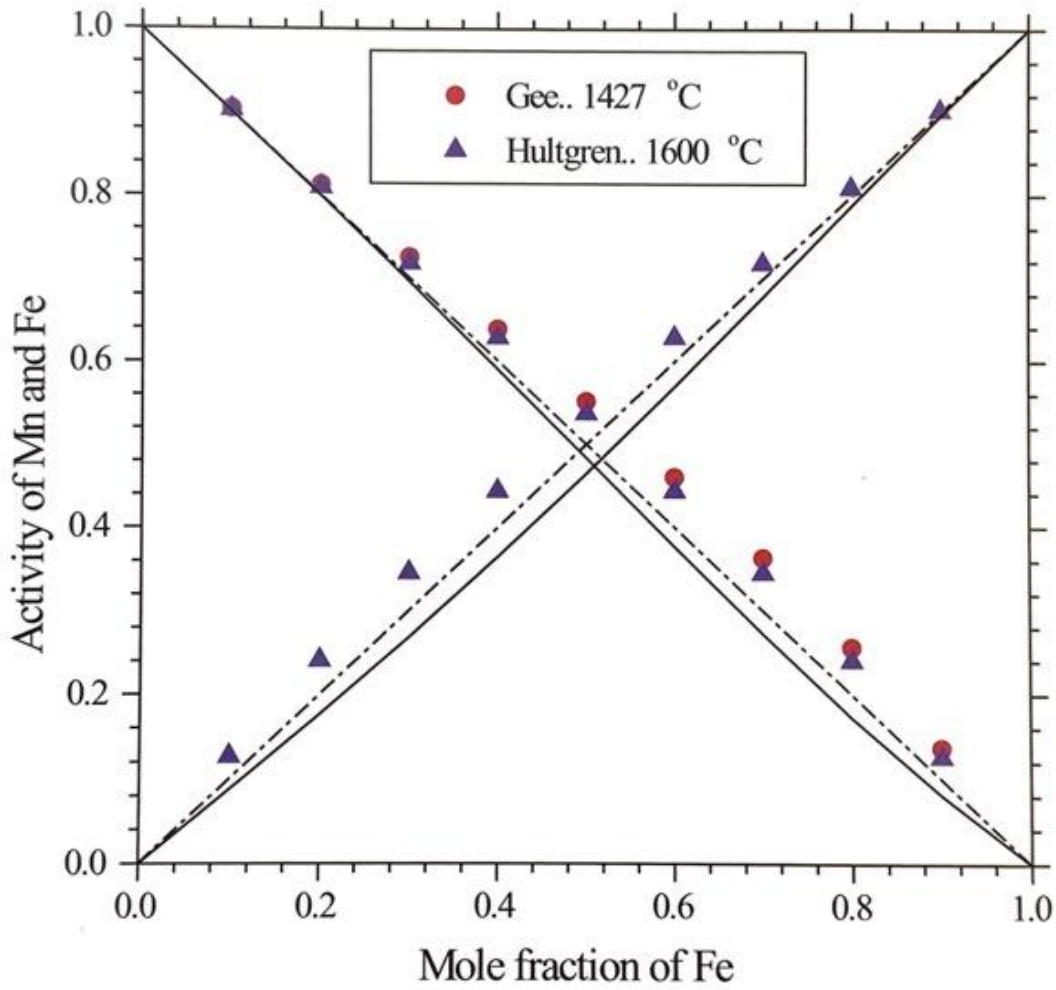


Figure 2-7: shows the activity of Mn and Fe by the mole fraction of Fe. The figure is obtained from [1] based on the studies from Gee et al. [18] and Hultren et al. [19].

2.5 Calcium-aluminat phase diagram

Studying the related phase diagrams for the HalMan process, which are calcium-aluminate and calcium-manganate slags, is crucially important, and the main binary and ternary slag systems are studied as follows.

The presented phase diagram for CaO-Al₂O₃ shown in Figure 2-8 gives the possible phases from 30-70wt% Al₂O₃ also including the semi-stable phase 12CaO•7Al₂O₃, denoted C12A7 [20].

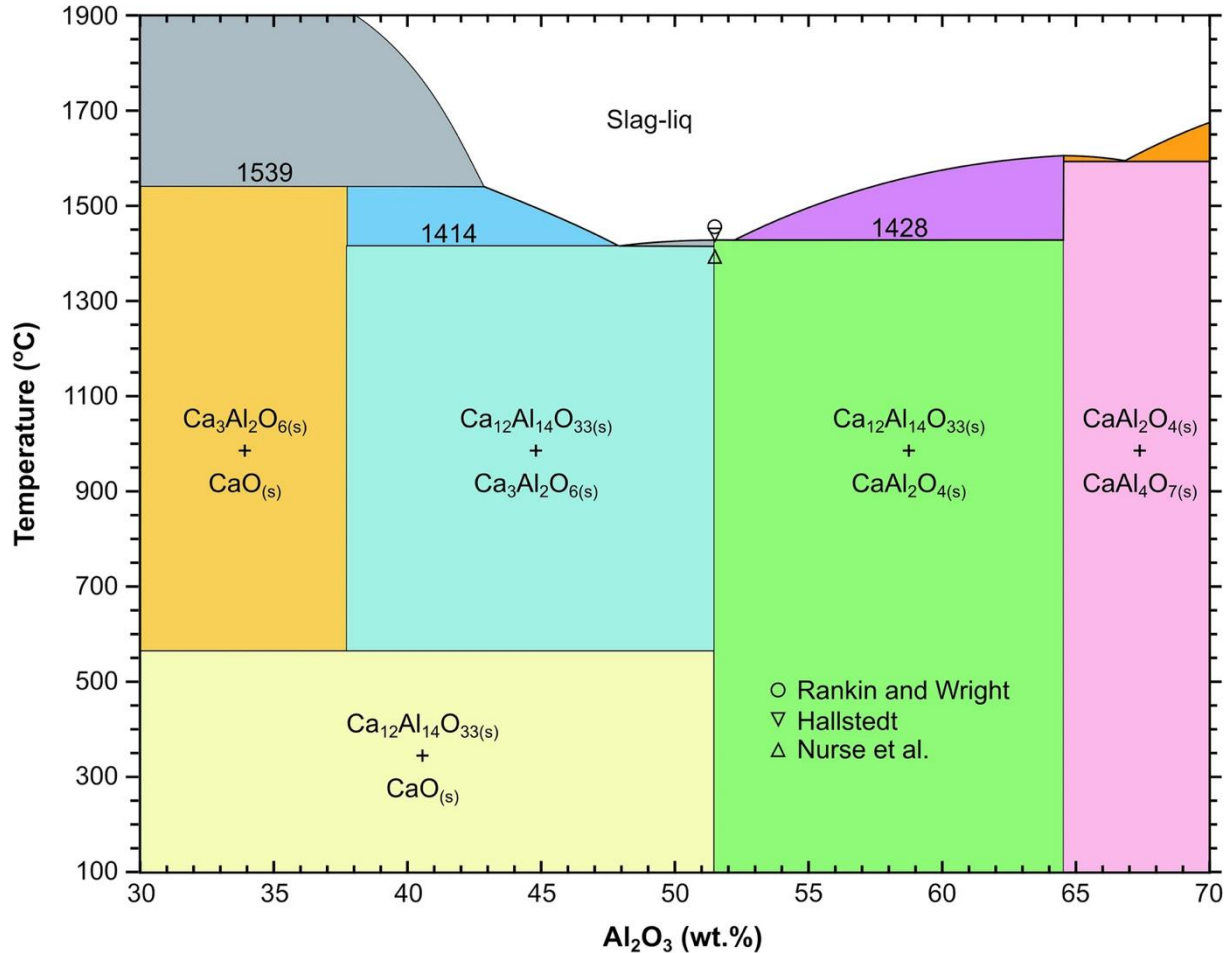


Figure 2-8: shows the binary CaO-Al₂O₃ system from 30-70wt% Al₂O₃ constructed using FactSage, which includes the C12A7 phase and its melting point according to Hallstedt [21] Nurse et al., [22] and Rankin and Wright [23].

Azof et al. [20] found that mayenite, C12A7, occurs at 770°C to 1390°C, and the melting point for the phase is at 1450°C for a mass ratio of 49:51 for CaO and Al₂O₃. The C12A7-phase is found to be interesting, as it is the most leachable Al₂O₃-CaO-phase according to [20], and is therefore interesting in terms of alumina recovery from the slag [17].

2.6 CaO-Al₂O₃-MnO

Figure 2-9 shows the ternary diagram for CaO-Al₂O₃-MnO, and possible phases present at 1400°C at 1atm.

$\text{Al}_2\text{O}_3 - \text{MnO} - \text{CaO}$, 1400°C, 1 atm

Data from FToxid - FACT oxide databases

FactSage

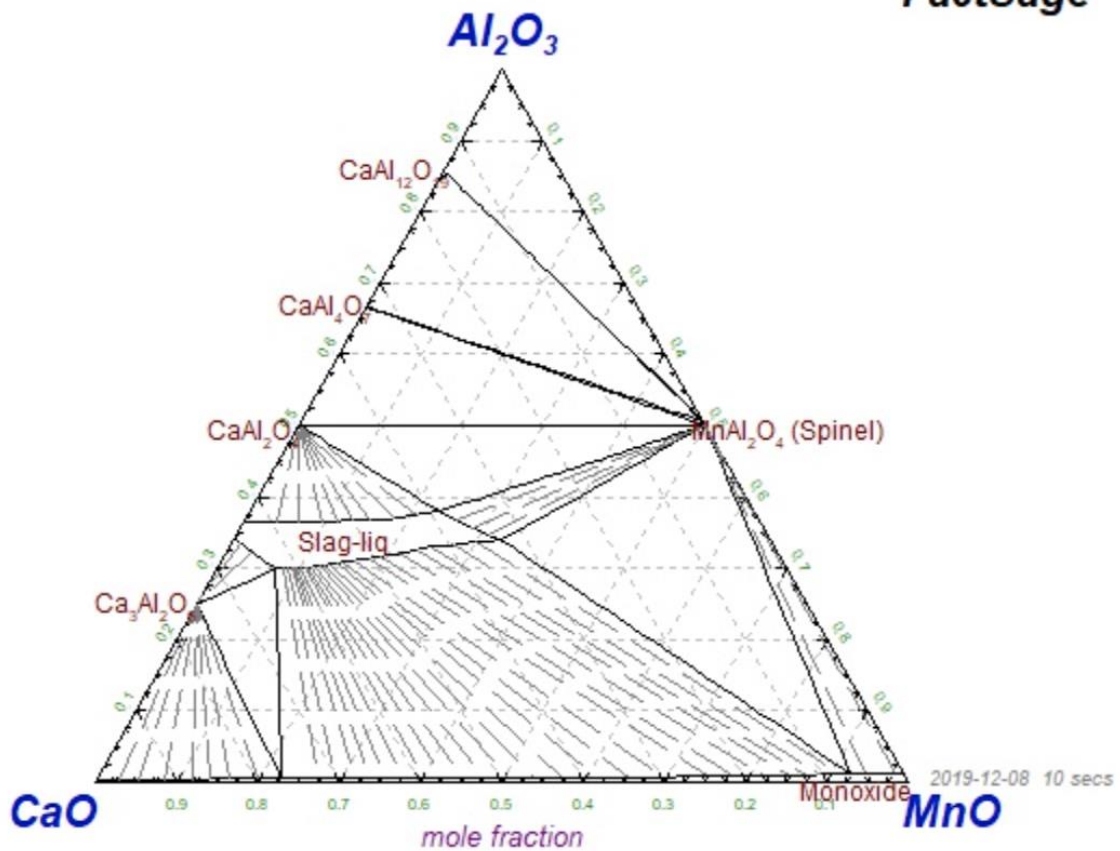


Figure 2-9: shows the phase diagram for $\text{Al}_2\text{O}_3\text{-MnO-CaO}$ at 1400°C from FactStage.

Figure 2-10 shows the phase diagram of CaO-MnO from FactStage with melting point for MnO at 1842°C and for CaO at 2572°C. In the system, MnO and CaO are completely miscible in both liquid and solid-state [1].

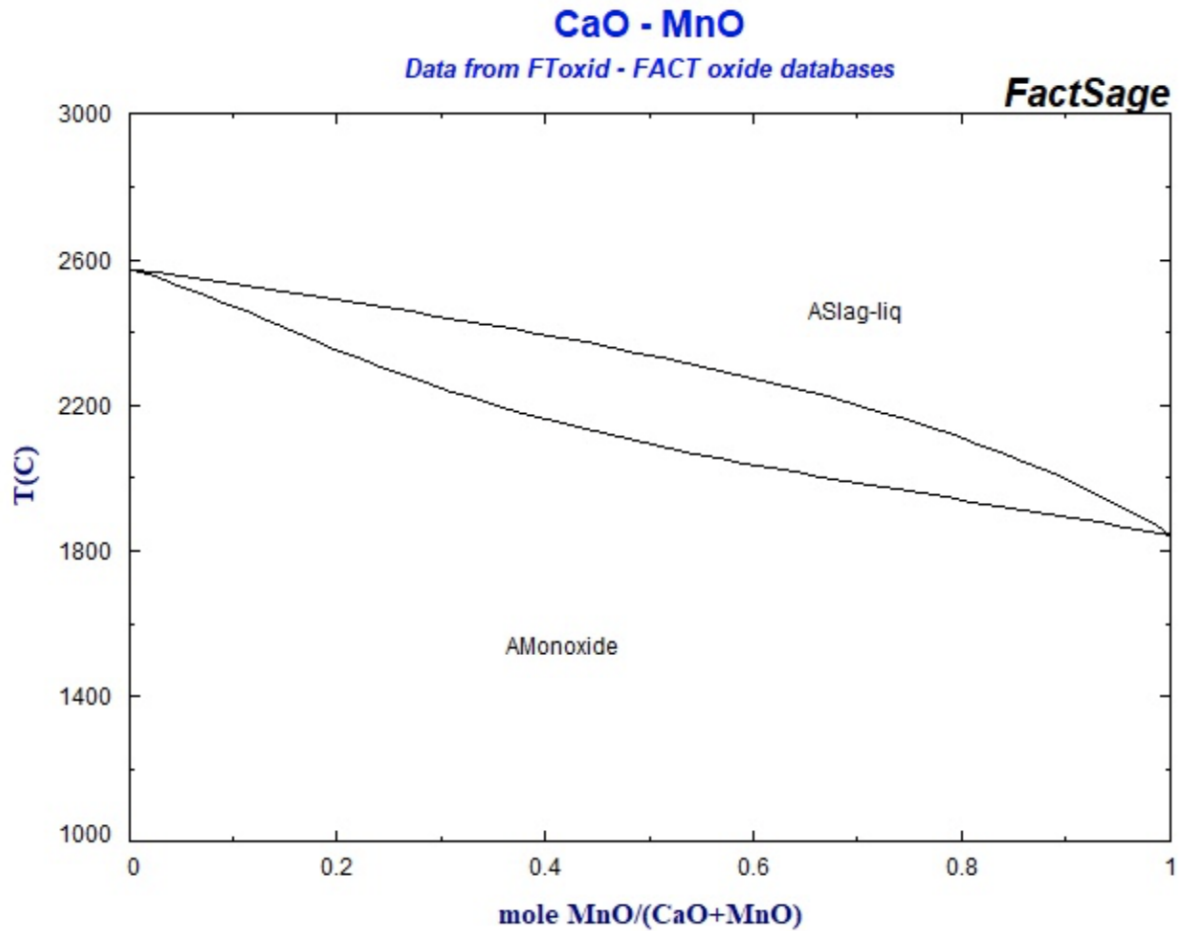


Figure 2-10: The phase diagram for CaO-MnO system.

2.7 Differential scanning calorimetry

A differential scanning calorimeter (DSC) specifically measures “the change of the difference in the heat flow rate to a sample and to a reference sample while they are subjected to a controlled temperature program” [24]. In a standard DSC, this is achieved by using thermocouples to measure the temperature difference between the sample and a standard sample. In this study, the isothermal mode is used where the heat flow and temperature are maintained in the sample. The change of heat flow will be zero, while the scanning mode changes the sample temperature linearly with time. [24]

DSC analysis outputs are usually represented as a curve where the heat flow rate is plotted against temperature. A positive change in heat flow, [mW], indicates exothermic behavior in the sample, while a negative indicates endothermic behavior. [24]

3. Methodology

This chapter gives an overview of the methods and experimental procedures used in this thesis.

3.1 Experimental procedure

Pre-reduced Mn ore by hydrogen (containing MnO and metallic iron) in dry form and a calcined lime (CaO) were separately milled to <500µm. The lime was kept in a desiccator to avoid oxidation caused by air moisture. A mixture of MnO and CaO was prepared for each smelting-reduction test based on the desired stichometry. As Figure 3-1 shows, DSC analysis, smelting, and smelting reduction with Al were performed, as well as characterization by SEM and XRD analysis.

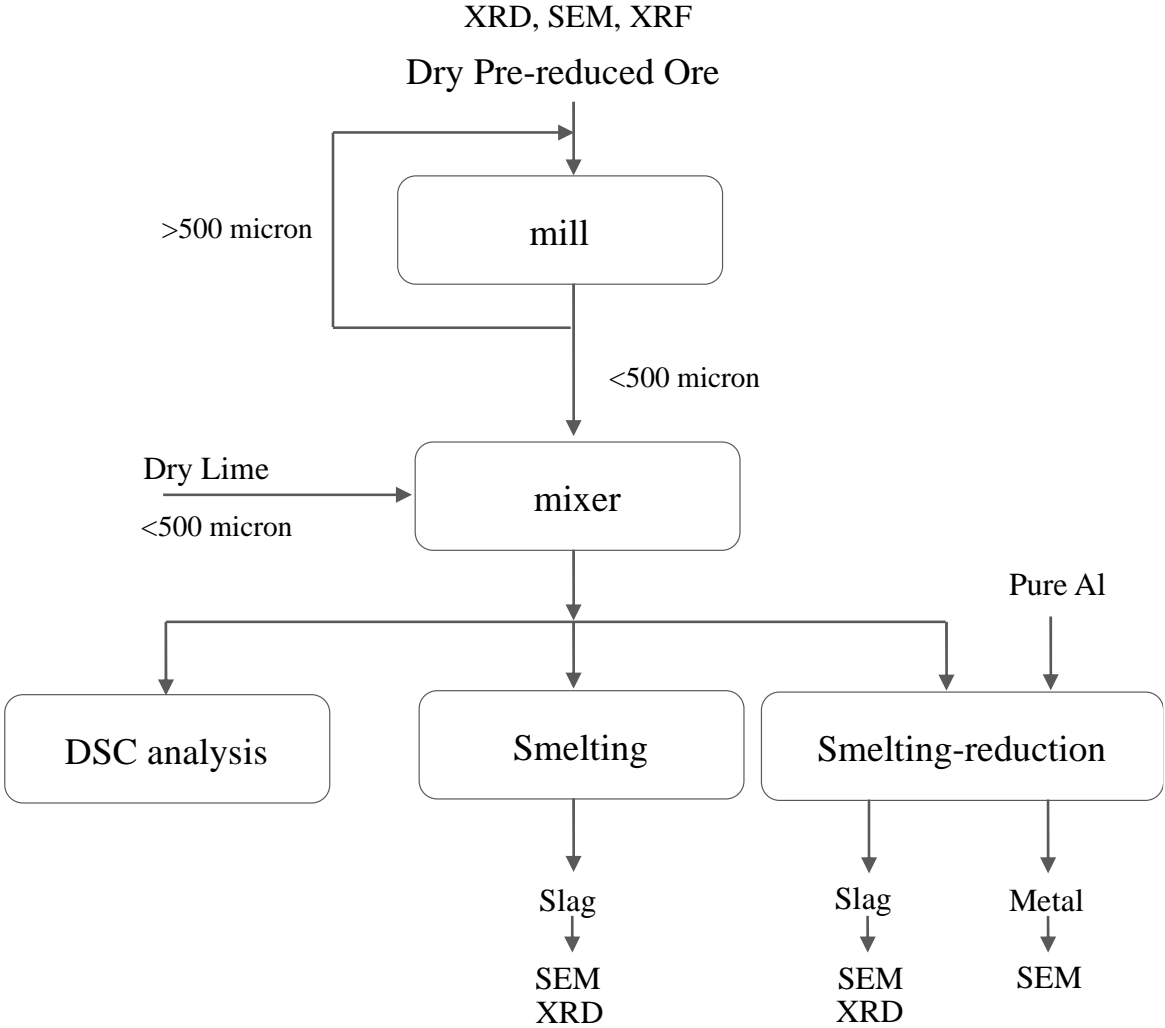


Figure 3-1: Schematic illustration of the experimental procedure and materials flow.

For the smelting-reduction with Al, the variables set was the temperature, processing time, and stoichiometric composition, as shown in Table 3-1. The sample names given in this table will be used throughout the thesis. The heating rate for all samples was 25°C/min.

Table 3-1: Experimental conditions and sample names for the samples undergoing the aluminothermic smelting-reduction.

Holding temperature [°C]	Holding time at target temperature[h]	Composition	Sample name
1300°C	1	1.0	13-1.0
1300°C	1	0.8	13-0.8
1400°C	1	1.0	14-1.0
1400°C	1	0.8	14-0.8
1500°C	1	1.0	15-1.0
1500°C	1	0.8	15-0.8
1500°C	0.5	1.0	15-0.5h
1500°C	1.5	1.0	15-1.5h

The compositions 1 and 0.8 is given based on the 100% and 80% stichometry of Al₂O₃ theoretically produced based on the MnO content in the samples and is discussed further in 3.2 Materials.

Table 3-2: Experimental details for samples in DSC/TG and smelting trials of pre-reduced ore-lime mixtures.

Equipment	Holding temperature [°C]	Holding time [h]	Composition	Sample name
DSC/TG	1500	1h	1.0	DSC-1.0
DSC/TG	1500	1h	0.8	DSC-0.8
Resistance tube furnace	1500	1h	1.0	Smelt-1.0
Resistance tube furnace	1500	1h	0.8	Smelt-0.8

3.2 Materials

The materials used in the experimental part of the work were pre-reduced Mn ore in which Mn is in the form of MnO and Fe is metallic, Lime (CaO) as flux, and pure aluminum (Al) metal. The Mn ore used was pre-reduced in H₂ atmosphere at 700°C-1000°C in the project work for the course TMT4500 and contains 67.83wt% MnO as seen in Table 3-3 [10]. The iron inclusion was yielded as metallic Fe at these conditions as indicated previously and is therefore given in the table in this form. **Feil! Fant ikke referanseilden.**

Table 3-3: Composition of pre-reduced Mn ore measured by XRF, given in weight percent.

Oxid	[wt%]	Oxid	[wt%]
CaO	6,90	K ₂ O	0,28
MgO	2,83	P ₂ O ₅	0,84
SiO ₂	4,99	SO ₃	0,16
Al ₂ O ₃	1,01	SrO	0,22
Fe	13,65	BaO	0,18
<u>MnO</u>	67,83	Cl	0,10
Cr ₂ O ₃	0,02	CeO ₂	0,21
TiO ₃	0,02	Na ₂ O	0,75

The lime used in the experimental work contained 90.20 wt% CaO as seen in Table 3-4.

Table 3-4: The composition of lime, CaO, measured by XRF.

Oxid	[wt%]
Al ₂ O ₃	0.16
CaO	90.20
Fe ₂ O ₃	0.08
K ₂ O	0.03
MnO	0.01
<u>MgO</u>	0.50
Na ₂ O	<0.03
P ₂ O ₅	0.01
SO ₃	0.24
SiO ₂	0.19
Ti ₂ O ₂	<0.01
LOI	8.45

Primary Al with 99.83% purity was used for the smelting-aluminothermic reduction. The Al metals also contained minor impurities of Fe and Si as shown in Table 3-5.

Table 3-5: Composition of Al used for smelting-aluminothermic reduction, measured by EDS analysis.

Element	[wt%]
Al	99.83
Fe	0.12
Si	0.04

Pre-reduced Mn ore, and lime (CaO) were milled to <500µm separately in a steel ring mill. The lime was kept in a desiccator to avoid oxidation caused by air moisture. A mixture of them was then prepared for each test based on the desired stoichiometries to reduce 100% or 80% of MnO from the pre-reduced ore. These are hereafter called series 1 and 0.8 The CaO addition depends on the theoretical amount of Al₂O₃ in the slag that is formed due to the aluminothermic

reduction of MnO in the two series. The calculated amounts of Al, and CaO needed for a 100g pre-reduced MnO ore is shown in Table 3-6.

Table 3-6: The theoretical amount addition of Al and CaO at 100% and 80% stoichiometry for a 100g sample of pre-reduced MnO-ore, all masses in g.

For 100 g reduced ore	Al needed	Al ₂ O ₃ produced	Total Al ₂ O ₃ in slag	CaO in final slag	CaO in ore	CaO needed	Lime needed
Series 1 (100% stoichiometric)	17.20	32.48	33.49	33.49	6.90	26.59	29.48
Series 2 (80% stoichiometric)	13.76	25.99	26.99	26.99	6.90	20.10	22.28

The complete calculations for the sample masses are given in Appendix 1, and the weighed-in masses for each sample is found in Appendix 2.

3.3 Sample preparation

For the smelting-reduction and smelting trials, the ratio of CaO and Al₂O₃ in the final slag was targeted to CaO/Al₂O₃=1.0 and CaO/Al₂O₃=0.8, based on the XRF analysis of the pre-reduced Mn ore and lime shown in the previous chapter.

For the smelting, the ore-lime mixture was placed in an alumina crucible with a thermocouple placed in the sample with a protective alumina tube around it to ensure the protection of the thermocouple as shown in Figure 3-2.

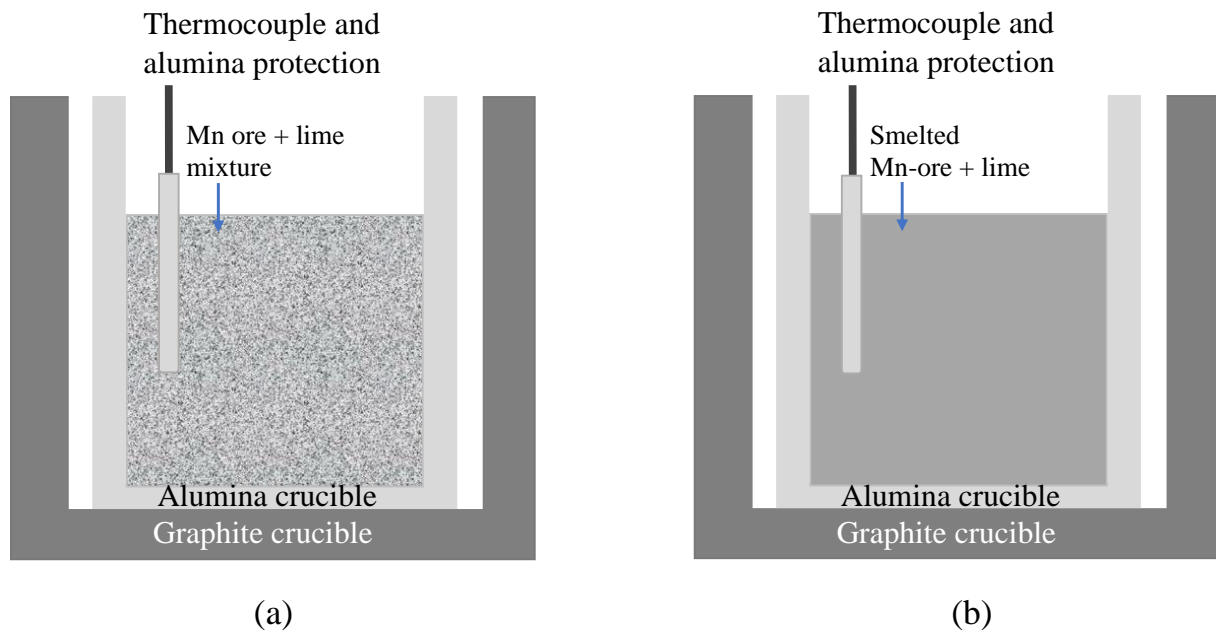


Figure 3-2: Schematic of the sample and crucible for the smelting trials. The setup and figures are inspired by [17].

A similar setup was used for the samples prepared for aluminothermic smelting-reduction, as seen in Figure 3-3. Here the MnO and CaO were mixed first, and Al was placed in the crucible. The sample mass was pressed together, and holes were made in the sample mass to allow gas to leave the sample.

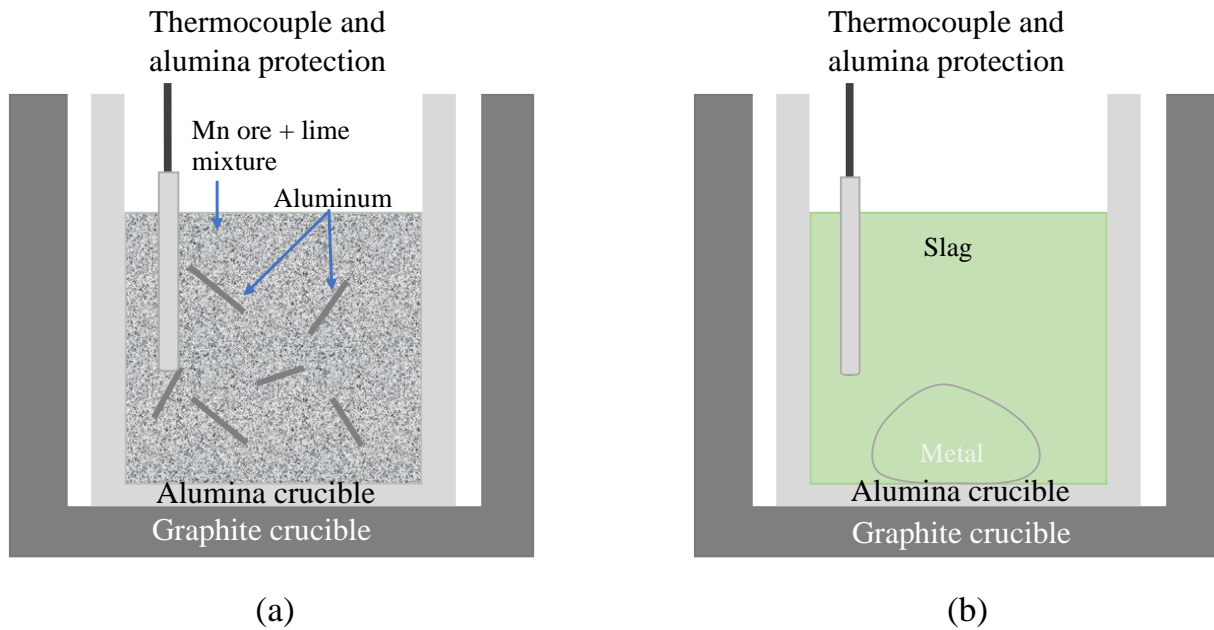


Figure 3-3: Schematic of the sample and crucible-for the samples undergoing aluminothermic smelting-reduction. The setup and figures are inspired by [17].

3.4 Furnace operation

The furnace used for the smelting and aluminothermic reduction was a tube furnace. The temperature of the furnace is controlled by the thermocouple in the wall and the thermocouple placed with the sample, and the furnace is heated by a graphite heating element. The prepared samples were placed in a graphite crucible and attached to the sample rod and placed in the furnace from the bottom and upwards. Before running the furnace, it was vacuumed and filled with Ar gas 2-3 times. During the experiment, the Ar gas flow was set to 1 liter per minute, and the pressure in the furnace to 1300 mbar to prevent air leakage into the furnace. A schematic drawing of the furnace with sample is shown in Figure 3-4.

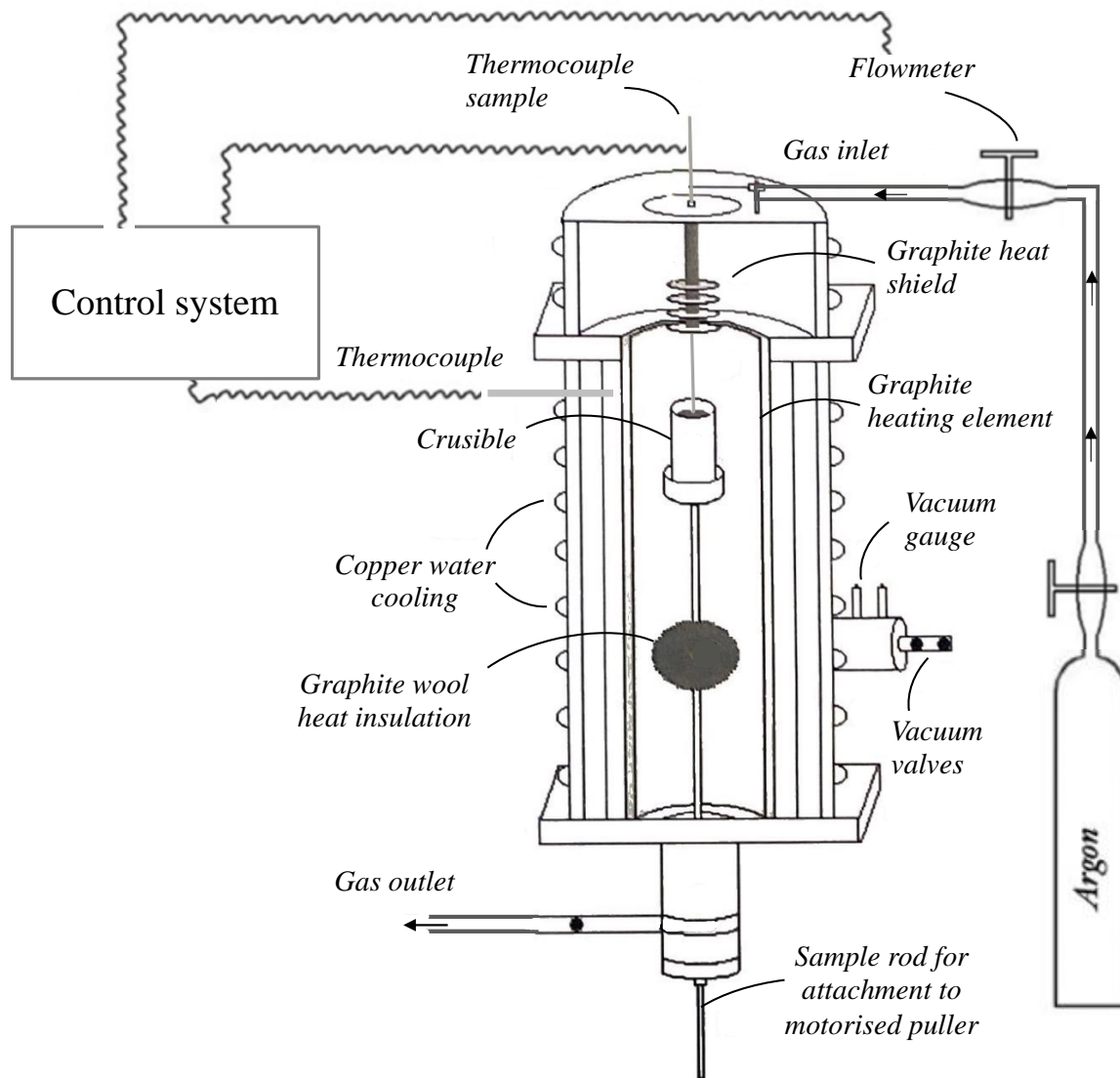


Figure 3-4: A schematic drawing of the tube furnace used for the smelting and smelting reduction trials.

The target temperatures for the samples were 1300°C, 1400°C and 1500°C and the program for the target temperature of 1500°C is given in Table 3-7 with a ramp rate of 25°C/min. The high-power limit used is based on experience from previous users of the tube furnace.

Table 3-7: The program used for the samples smelted and reduced at 1500°C.

Time interval	End temp.	Ramp rate	MFC (Ar)	High power limit
[min]	[°C]	[°C/min]	[l/min]	[%]
12	300	25	1	30
12	600	25	1	40
16	1000	25	1	60
10	1250	25	1	70
8	1450	25	1	80
60	1500	-	1	80
-	25	-	1	0

3.5 Microstructural analysis

To investigate properties in SEM and EDS, samples of the slag and the metal from the aluminothermic reduction were prepared by mounting them into a resin and polished using a Struers Tegamin-30. The mounted samples were covered with aluminum foil, and carbon tape was used between the foil and the sample surface to ensure electrical contact, the samples were then coated with carbon to ensure electrical contact with the entire sample surface.

The microstructure of the different samples was examined in SEM, run with a Hitachi S-5500 using 15 kV acceleration voltage. Pictures of the surface were taken from 100x to 4000x magnifications.

3.6 Phase analysis

The XRD analysis was performed on the produced slags from the aluminothermic reduction experiments. One XRD sample was prepared from the calcinated ore in a muffle furnace and

one sample from each pre-reduced ore sample. All these samples were prepared from a portion of the samples via milling in a ring mill mentioned above. The obtained fine powders were then put in the dedicated XRD sample holder.

The instrument used was the D8 ADVANCE DaVinci with $\text{CuK}\alpha$ radiation for 30 minutes, $10-80^\circ$, and slit size 0.2. The results from the analysis were processed using the software DEFFRAC.EVA.

Mapping and point analysis were done by EDS in SEM. This was done for all samples at 4000x magnification and at a working distance of 10.

3.7 Differential scanning calorimetry

Initially, Differential thermal analysis (DTA) was planned for investigating thermal properties, such as the smelting point, of the ore with CaO addition. Due to technical problems, DTA analysis was not available during the project period. DSC was therefore performed to acquire some thermal data for the samples. Two samples with MnO and CaO were prepared for DSC analysis. To ensure that no reaction occurred between the sample mass and crucibles platinum crucibles, shown in Figure 3-5 (a) were used for the analysis. The setup for the crucible and sample for DSC is seen in (c), where the white crucible is a reference sample.



(a)

(b)

(c)

Figure 3-5: The platinum crucibles used, (a), crucible loaded with the sample, (b), and crucible with the sample prepared for analysis, (c), with DSC.

The samples were heated to 1500°C with a ramp rate of 25°C/min as seen in Table 3-8, similar to the samples smelted in the resistance tube furnace.

Table 3-8: The temperature program used for DSC and TG analysis is shown in the table.

Temperature [°C]	Temperature rate [°C/min]	Holding time [min]	Total time per step [min]
25 → 1500	25	-	59
1500	-	60	-
1500 → 25	25	-	59

4. Results

4.1 Flux-smelting behavior of the pre-reduced ore

4.1.1 Differential scanning calorimetry

DSC was performed on two samples, one with 1 molar relationship and one with 0.8 molar for $\text{CaO}/\text{Al}_2\text{O}_3$. The results of the DSC analysis are displayed in Figure 4-1. Both samples show somewhat similar behavior with temperature changes, and a sharp drop of power flow at about 400 °C is observed. A new peak is detected for both samples at about 1100°C, followed by a voltage drop with increasing temperature, and a new peak again at the setpoint of 1500°C is appeared. Throughout the holding period, the DSC value increases slightly for both samples.

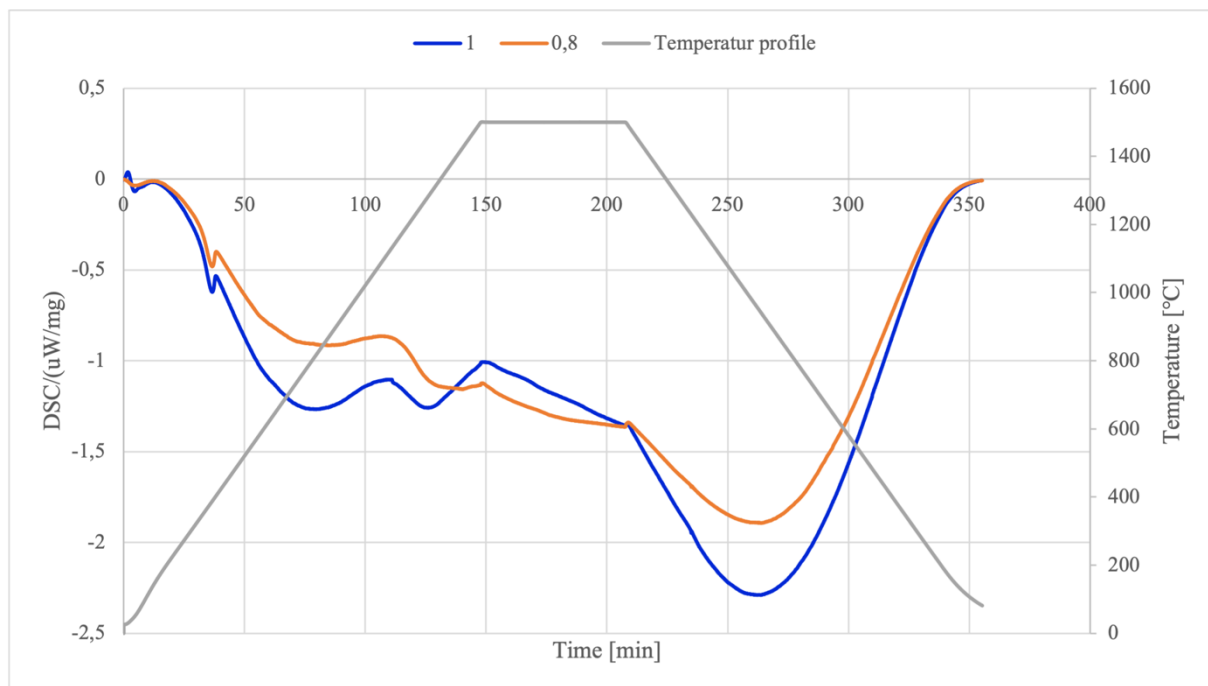


Figure 4-1: The DSC curves smelted MnO-CaO with 1 and 0.8 molar for $\text{CaO}/\text{Al}_2\text{O}_3$.

It was observed that the samples shrank into a pellet-like form after DSC analysis as seen in Figure 4-2, and both samples were sintered to the crucible.



Figure 4-2: Photo of the sample with 1 molar ratio of $\text{CaO}/\text{Al}_2\text{O}_3$ after DSC.

4.1.2 Microstructure of flux-smelted pre-reduced ore

The smelted pre-reduced ore-lime mixture of $\text{CaO}/\text{Al}_2\text{O}_3=1.0$ shows three clear phases, as seen in Figure 4-3. Fe is present in the phase formed as small spherical particles, close to a larger area phase, also spherical, mainly containing Mn and O. Fe, Ca, and Mg was also present. The third phase contains Ca, O, and Al and Si.

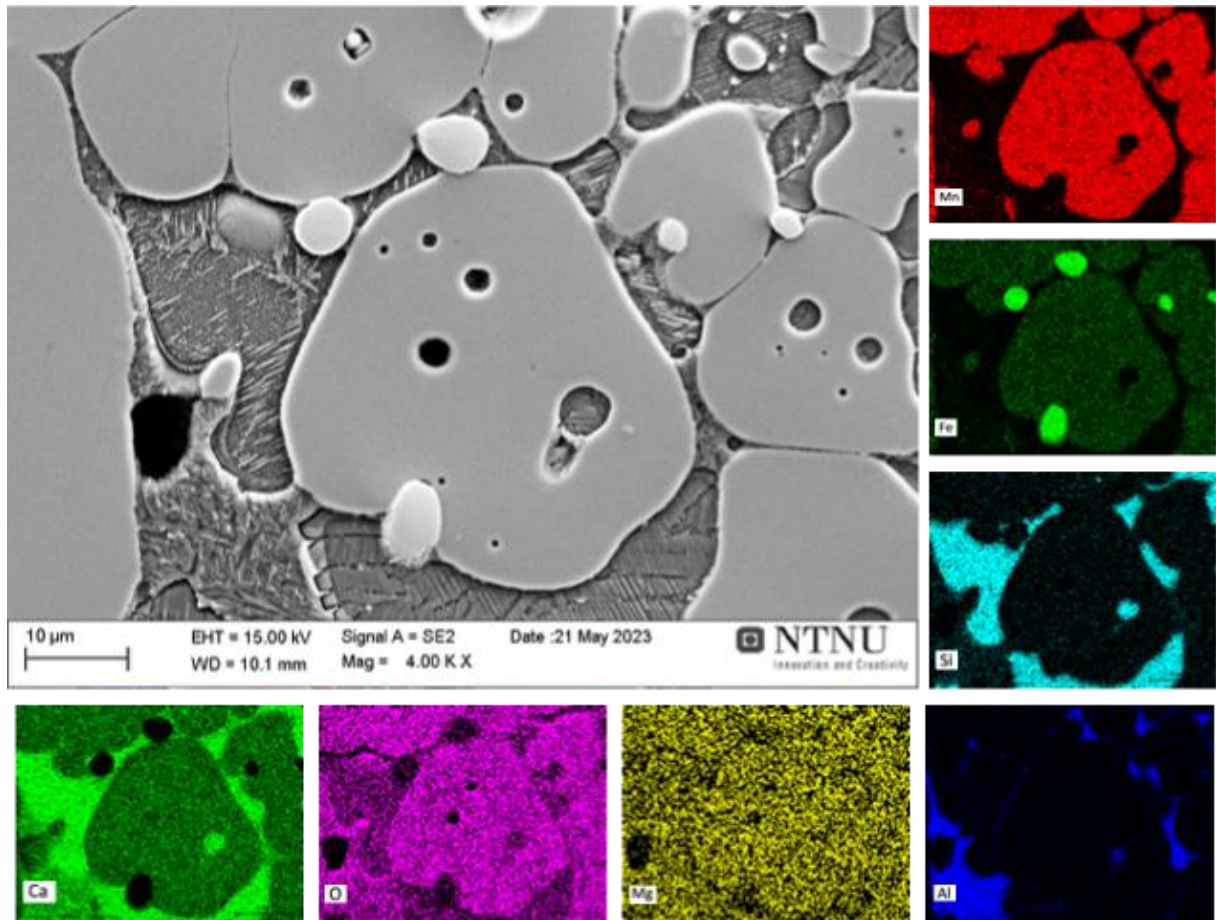


Figure 4-3: Microstructure and EDS mapping of MnO-CaO in 1 molar relationship

For the smelted pre-reduced ore-lime mixture of $\text{CaO}/\text{Al}_2\text{O}_3=0.8$ only two phases were detected as seen in Figure 4-4. The light phase contains Fe, with some O, Al, and Mg present. The darker phase contains Mn and Ca together with O. Mg, Al and Si is also detected here.

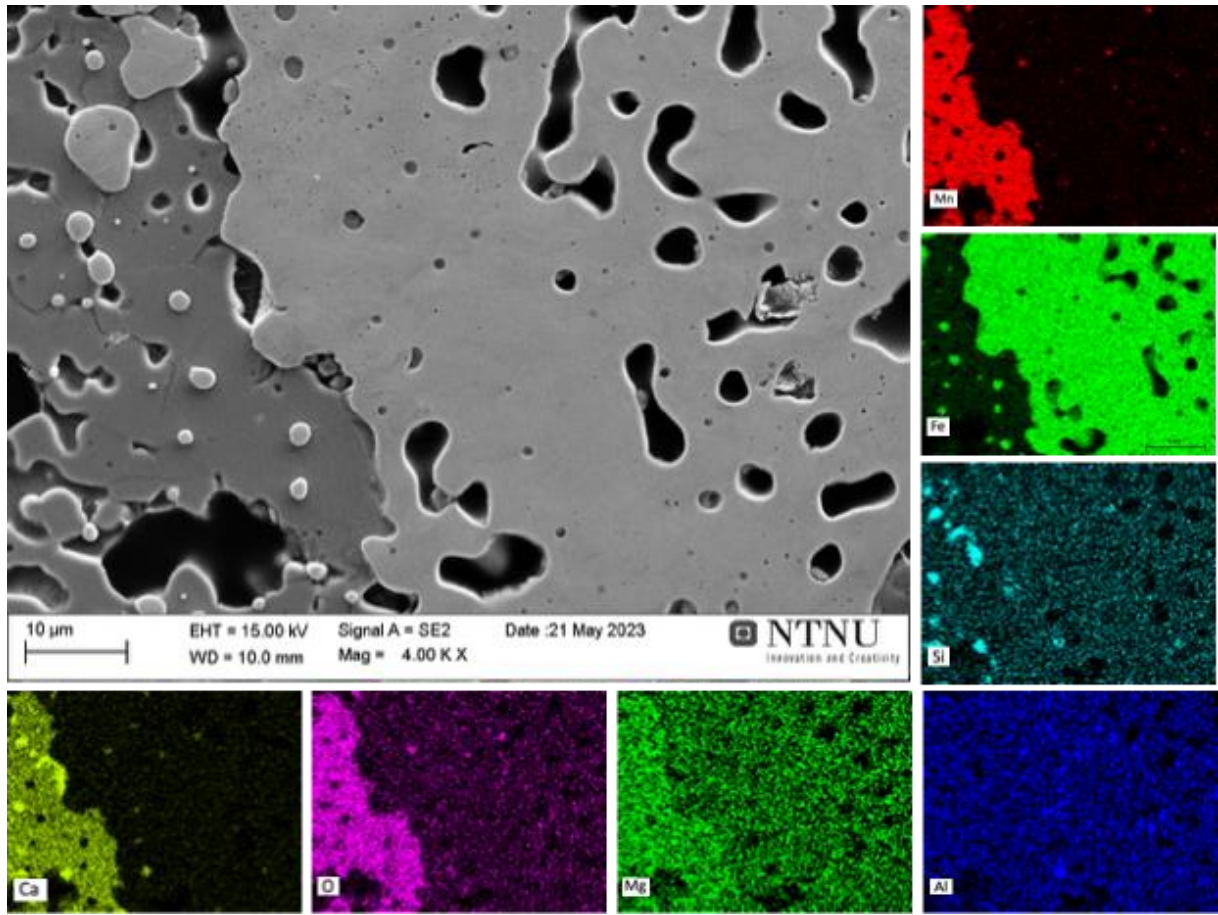


Figure 4-4: Microstructure and EDS mapping of MnO-CaO in 0.8 molar relationship

4.1.3 Phase analysis of the smelted pre-reduced ore

Figure 4-5 shows data from XRD analysis of the smelted pre-reduced ore-lime mixtures. Similar phases were detected at both CaO/Al₂O₃ ratios, but a minor phase of CaAl₂O₄ was detected in the 1 molar phase, where more lime was added.

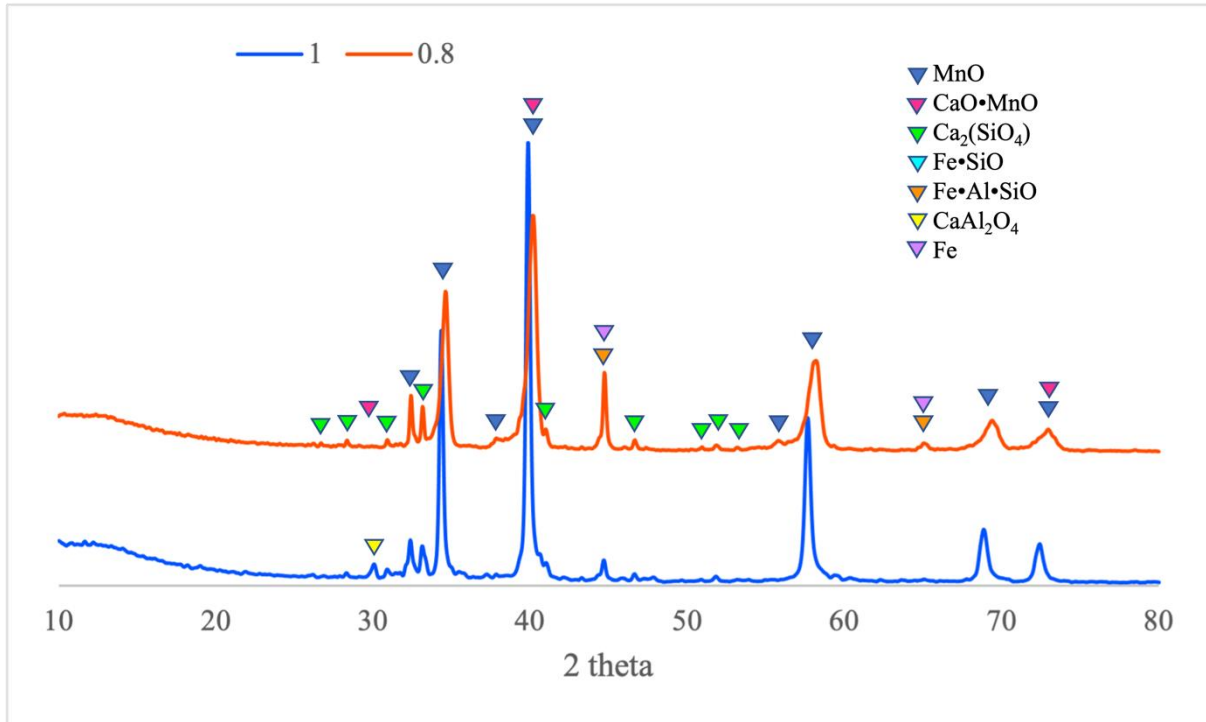


Figure 4-5: XRD pattern of smelted pre-reduced ore-lime mixtures.

The three phases found in the 1 molar pre-reduced ore-lime mixture were investigated further by point and area analysis from several areas around the sample surface, and Figure 4-6 shows typical results.

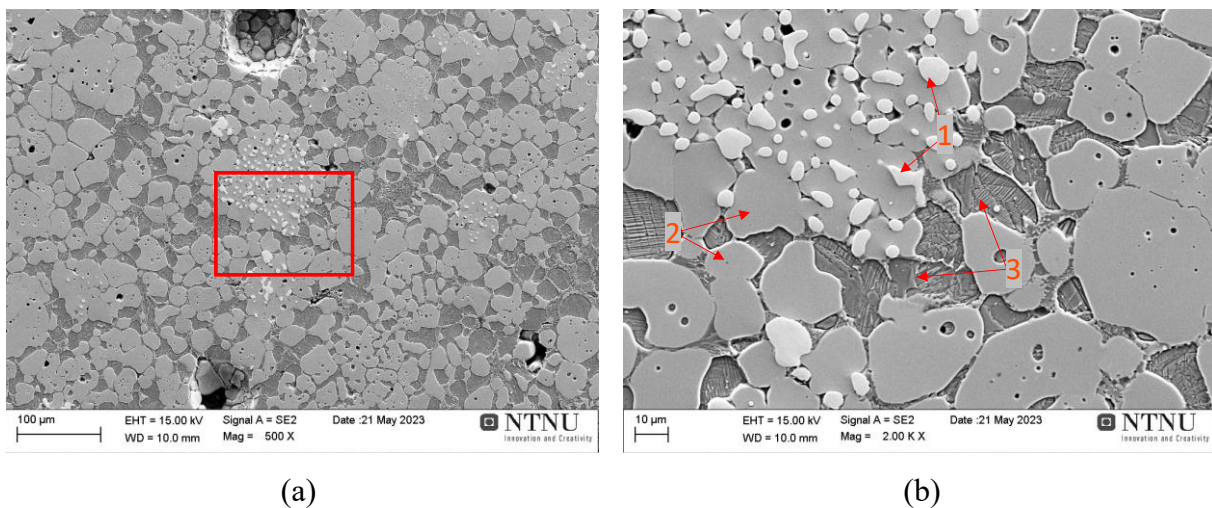


Figure 4-6: EDS areas analyzed from the smelted ore-lime mixture in $\text{CaO}/\text{Al}_2\text{O}_3=1$.

Table 4-1 shows the results from the point and area analysis of the points indicated in Figure 4-6. The raw data in the EDS analysis are elemental, hence the elements expected in oxide form were converted into oxide form regarding the XRD analysis results, and all values were normalized. Area 1 mainly contained Fe, area 2 had a high concentration of MnO, with Fe and CaO. The third phase mainly contained CaO and also Al₂O₃.

Table 4-1: The oxides/elements analyzed in the areas given in 6.

Oxides/elements	Phase 1	Phase 2	Phase 3
MnO	0.40	48.77	4,57
Fe	98.11	15.72	2.31
CaO	0.72	11.26	58.77
SiO ₂	-	0.07	13.31
MgO	-	3.18	0.25
Al ₂ O ₃	-	0.05	20.01
K ₂ O	-	0.09	0.64
P	-	0.00	0.13

The two phases found in the CaO/Al₂O₃=0.8 molar pre-reduced ore-lime mixture were also investigated further by point and area analysis from several areas around the sample surface, and Figure 4-7 shows the results.

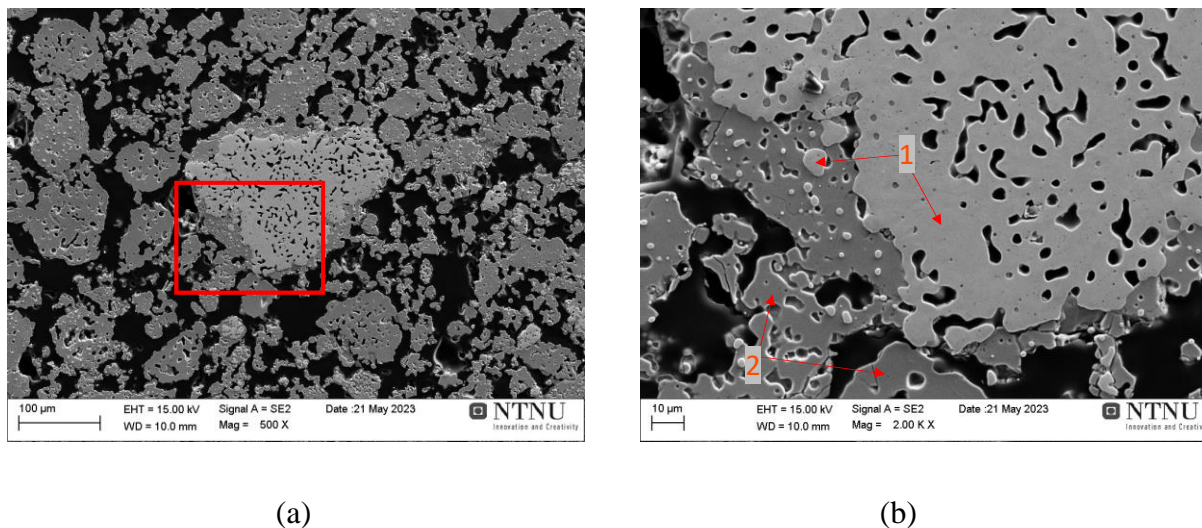


Figure 4-7: The areas analyzed insmelted pre-reduced ore-lime with CaO/Al₂O₃ = 0.8 .

Table 4-2 shows the results from the point and area analysis. The raw data in the EDS analysis are elemental, hence the elements expected in oxide form were converted into oxide form, and all values were normalized. Phase 1 mainly contained Fe, while phase 2 mainly contains MnO and CaO.

Table 4-2: shows the oxides/elements for 0.8 MnO-CaO in the areas given in Figure 4-7

Oxides/elements	Phase 1	Phase 2
MnO	0.82	71.42
Fe	98.38	7.38
CaO	0.64	19.70
SiO ₂	-	0.23
MgO	-	0.97
Al ₂ O ₃	-	0.12
K ₂ O	-	0.17
P	-	0.00

4.1.4 Mass loss and visual observations

The mass reduction of samples during the analysis was obtained by TG curves shown in Figure 4-8. It was found that the sample with a 1 molar ratio of CaO/Al₂O₃ achieved a weight reduction of 1.16% while the 0.8 molar ratios of CaO/Al₂O₃ achieved 1.34% weight reduction. The largest drop in the TG-curves was observed around 400°C. During cooling, a spike is observed for both samples at 1200°C.

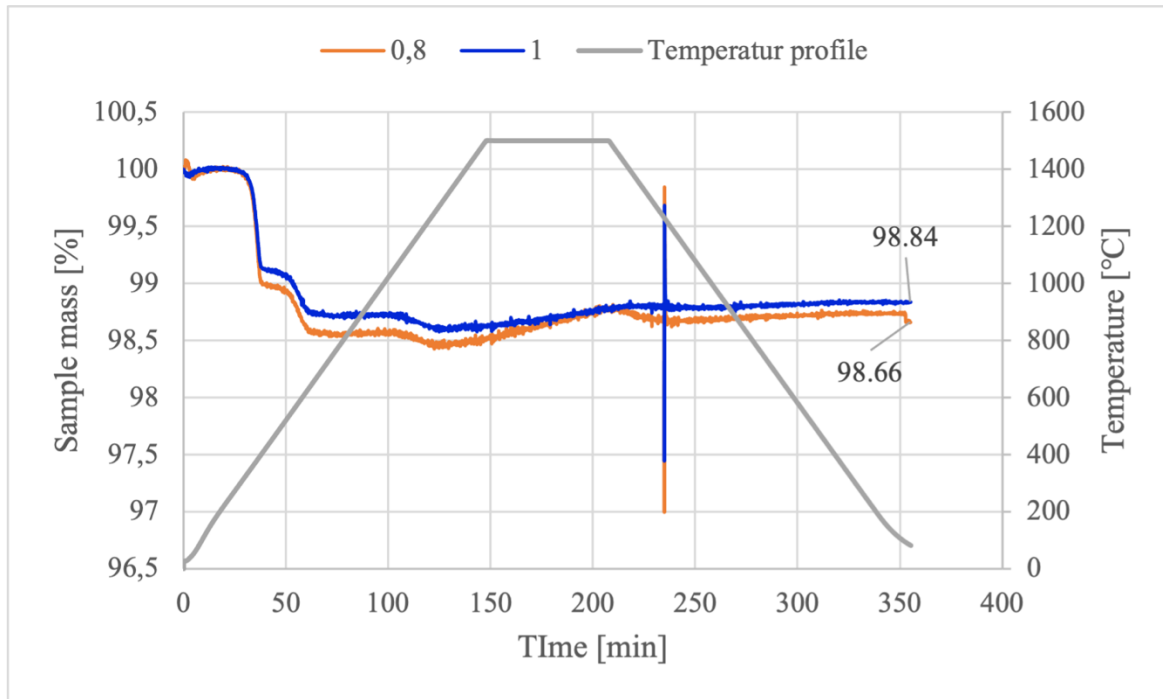


Figure 4-8: The TG curves from the DSC analysis is presented for samples with 1 and 0.8 molar for $\text{CaO}/\text{Al}_2\text{O}_3$.

The mass loss after smelting in a tube furnace is given in Table 4-3 and was found to be 0.6wt% for the $\text{CaO}/\text{Al}_2\text{O}_3=1$ molar ratio and 0.71wt% for the $\text{CaO}/\text{Al}_2\text{O}_3=0.8$ ratio.

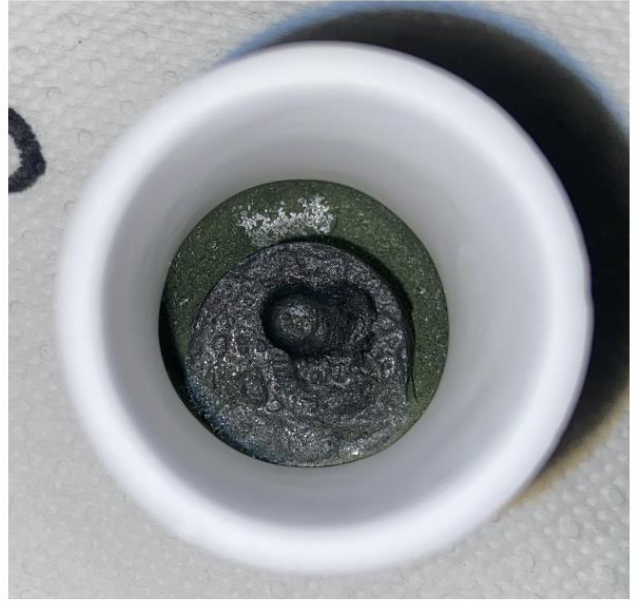
Table 4-3: Mass loss of smelted pre-reduced ore-lime mixtures

Sample	Mass loss [g]	Mass loss [wt%]
MnO-CaO 1	0.21	0.66
MnO-CaO 0.8	0.24	0.71

Figure 4-9 shows the samples after smelting in alumina crucible in the tube furnace. It was observed that both samples shrank in size and formed a large single pellet-like shape, and the samples were sintered ore gotten semi-molten. The surface of the samples was somewhat different, the $\text{CaO}/\text{Al}_2\text{O}_3=1$ ratio pellet had a shiny surface, and some green residue was left at the bottom of the crucible. One side of sample was stuck to the crucible as seen in picture (b). The 0.8 ratio sample had a more powdery-looking surface and was easily removed from the crucible, obviously indicating less sintering/melting. There was no green residue in this crucible.



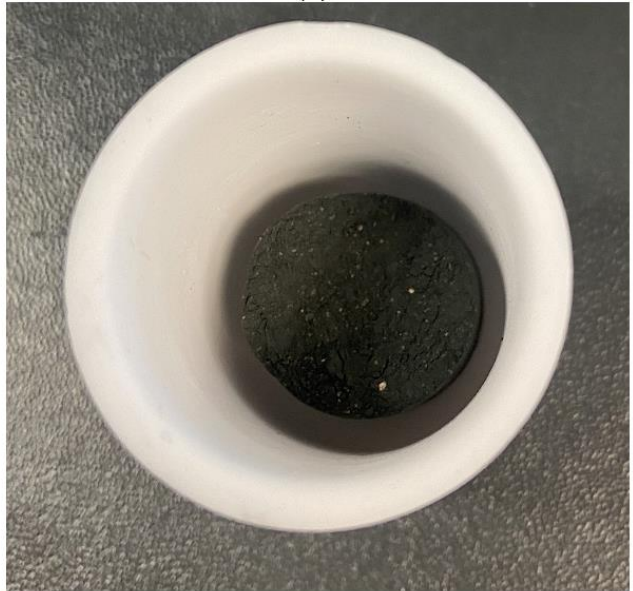
(a)



(b)



(c)



(d)

Figure 4-9: The smelted pre-reduced ore-lime samples, where (a) and (b) is the 1 molar relationship and (c) and (d) shows the 0.8 molar target $\text{CaO}/\text{Al}_2\text{O}_3$.

4.2 Aluminothermic smelting-reduction of pre-reduced ore

4.2.1 Microstructural analysis

Figure 4-10 (a) shows an overview picture of the sample surface with a metal phase surrounded by slag, and the alumina crucible to the right. In picture (b) the microstructure of the slag can be studied more closely. Two clear phases, one dark, and one light, are observed.

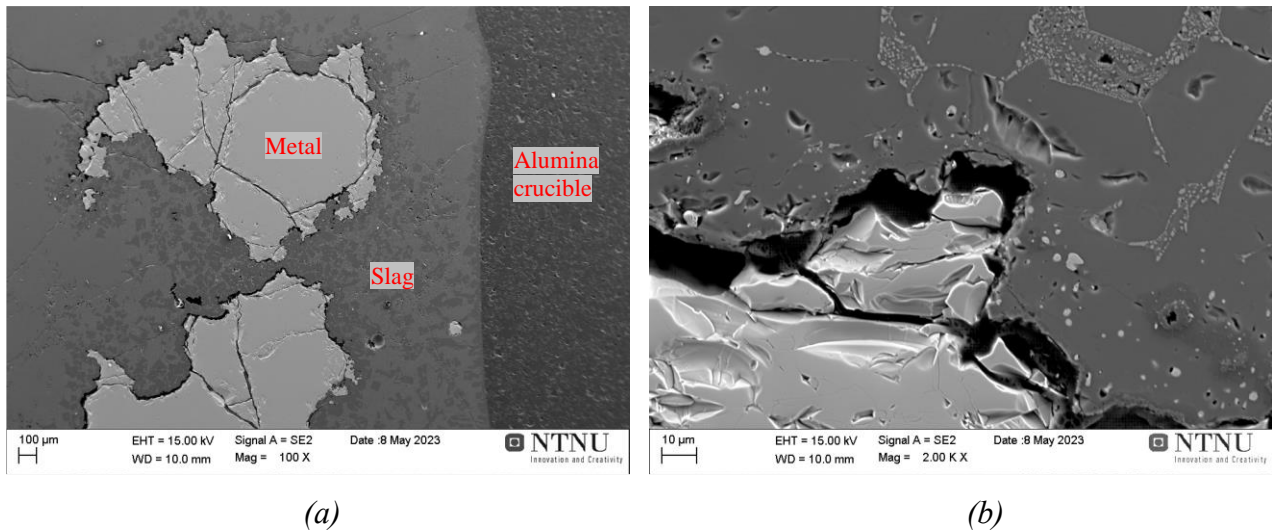


Figure 4-10: The microstructure of 13-1.0 sample at 100x, (a), and 2Kx, (b).

In Figure 4-11, mapping of an area with metal and slag phases is given. The metal phase contains Fe, Mn, and Si. The slag phase consists of Al and Ca with oxygen. The brighter ting phase in the slag contains similar elements as the metal phase.

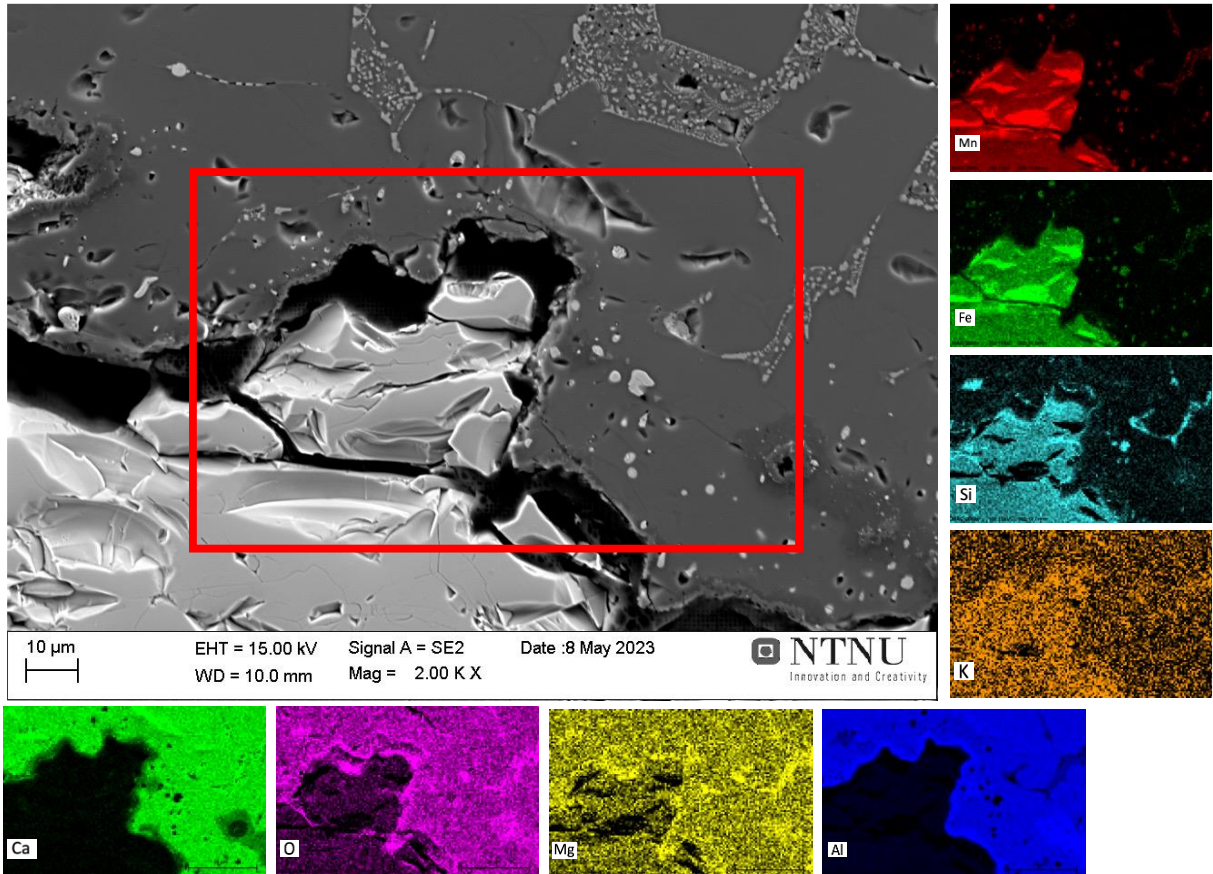


Figure 4-11: Elemental EDS mapping of metal and slag in sample 13-1.0.

Figure 4-12 two phases are observed in the slag for the 13-0.8 sample at 500x magnification. The phases can be more clearly observed in picture (b).

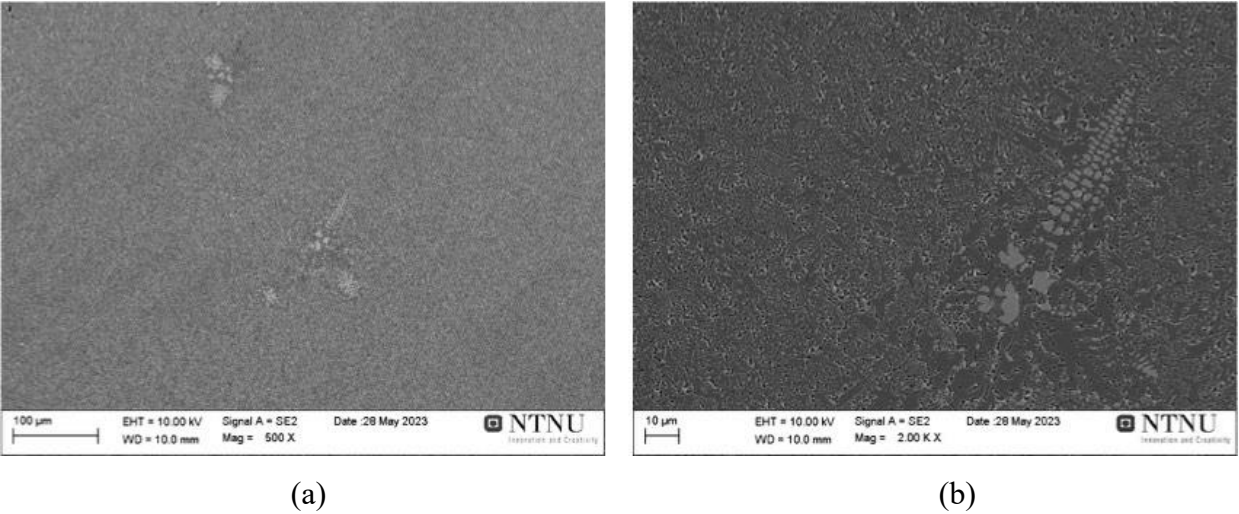


Figure 4-12: The microstructure of slag sample from 13-0.8 sample.

Figure 4-13 shows the EDS mapping of the phases observed in

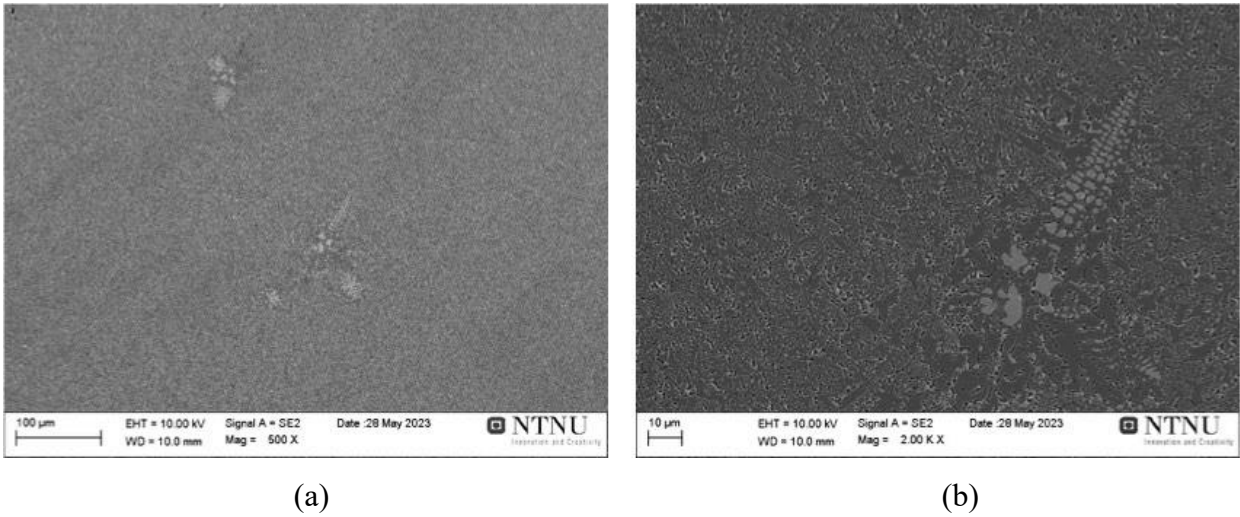


Figure 4-12. In the bright phase, Mn and Fe are observed. The surrounding phase contains Al and Ca. Oxygen, Si, and Mg were found in both phases.

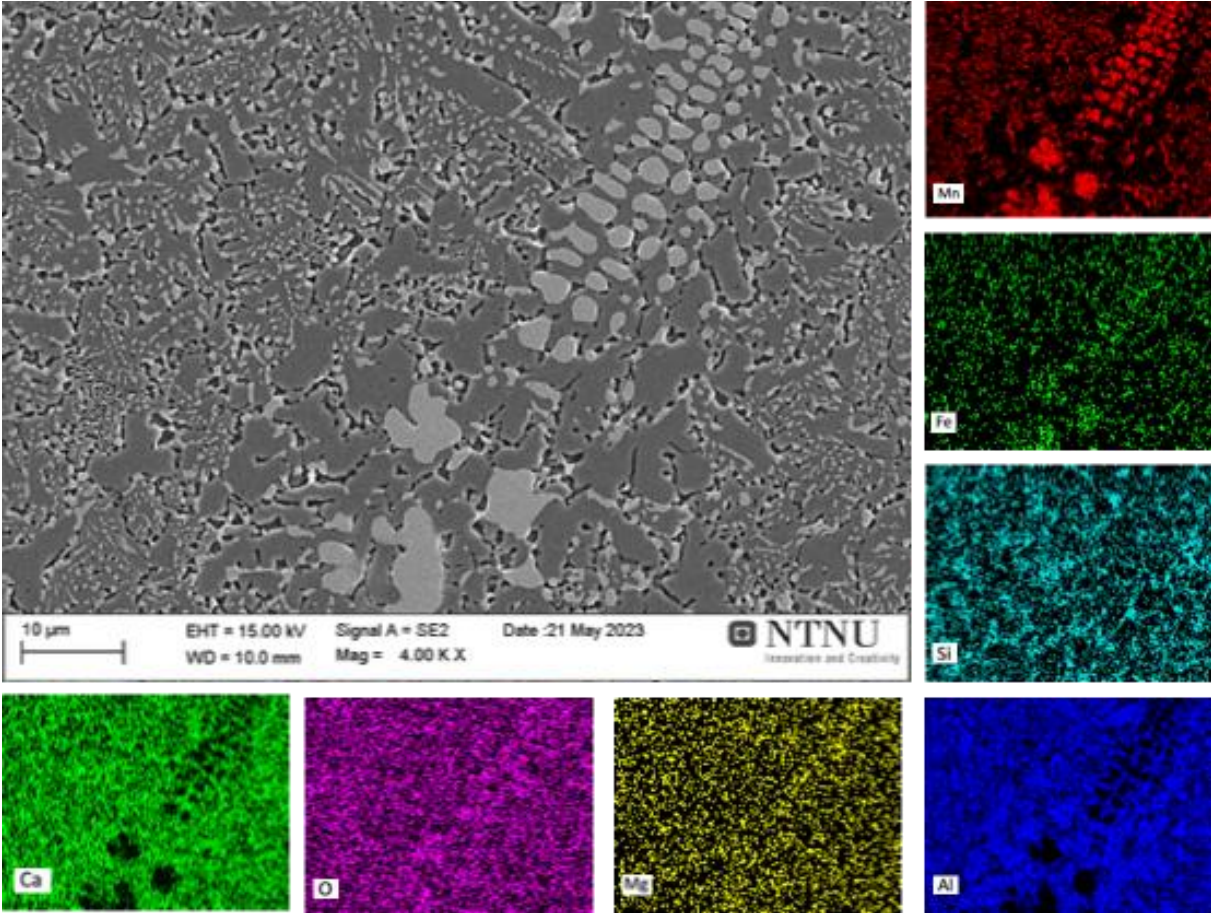
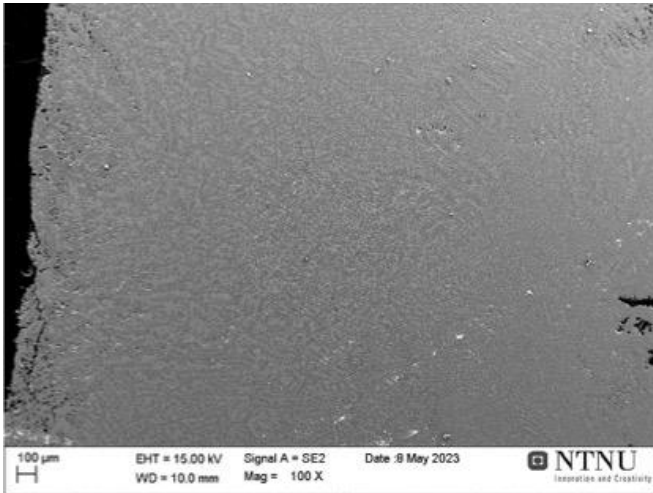
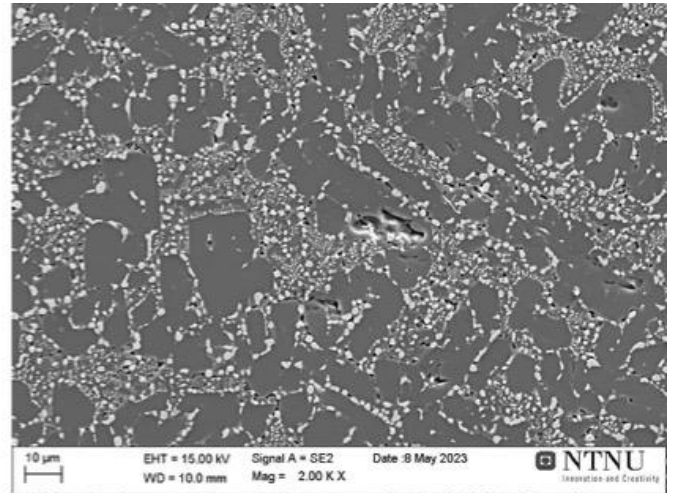


Figure 4-13: Elemental EDS mapping of slag phase for sample 13-0.8

Figure 4-14 shows an area of the slag phase for the 14-1.0 sample. In the picture (b) two phases are observed.



(a)



(b)

Figure 4-14: The 14-1.0 sample microstructure.

The two phases in 14-1.0 sample analyzed with EDS mapping show that the light phase contains Mn, Fe, and Si. In the darker phase Al is observed, Ca is present in both of the dark phases, shown in Figure 4-15.

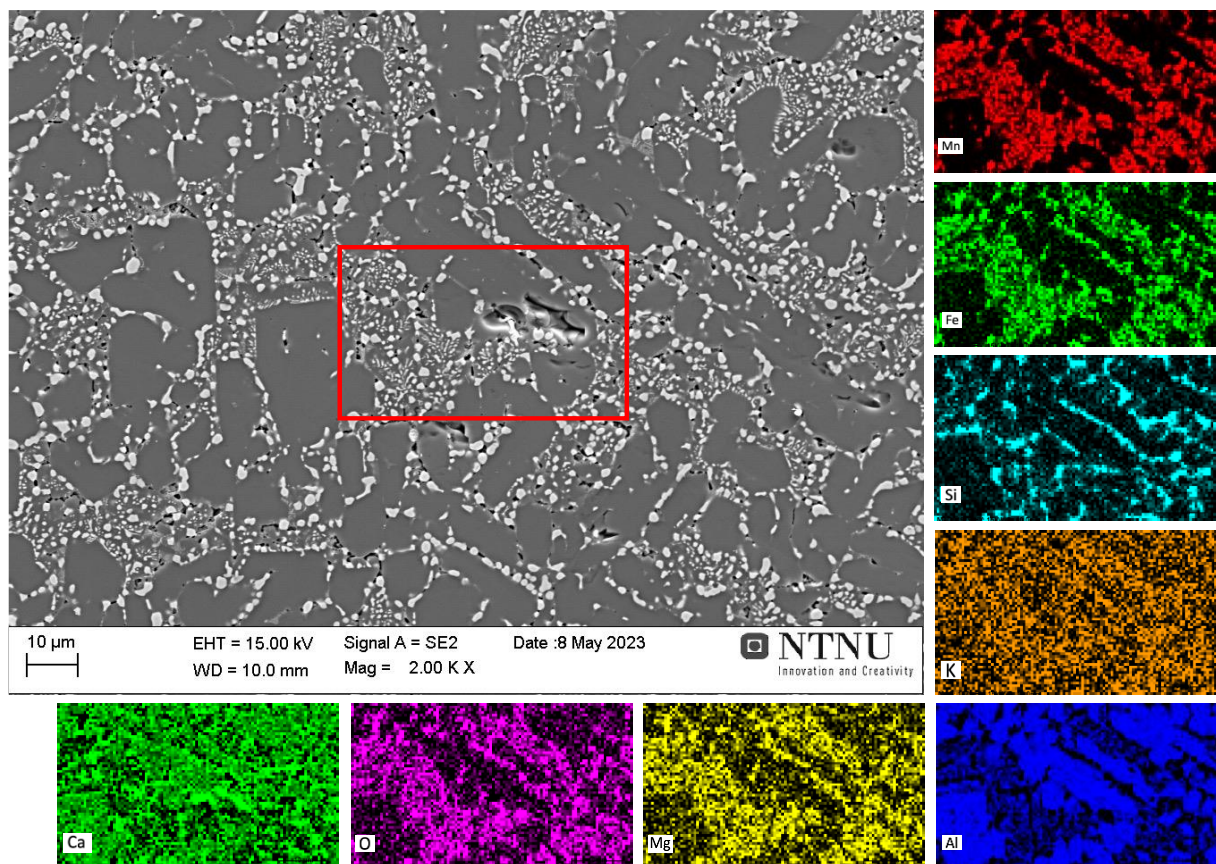


Figure 4-15: Elemental EDS mapping of sample 14-1.0.

The metal and slag phases in 14-0.8 are shown in Figure 4-16. Here the slag contains three phases with regard to the contrast differences.

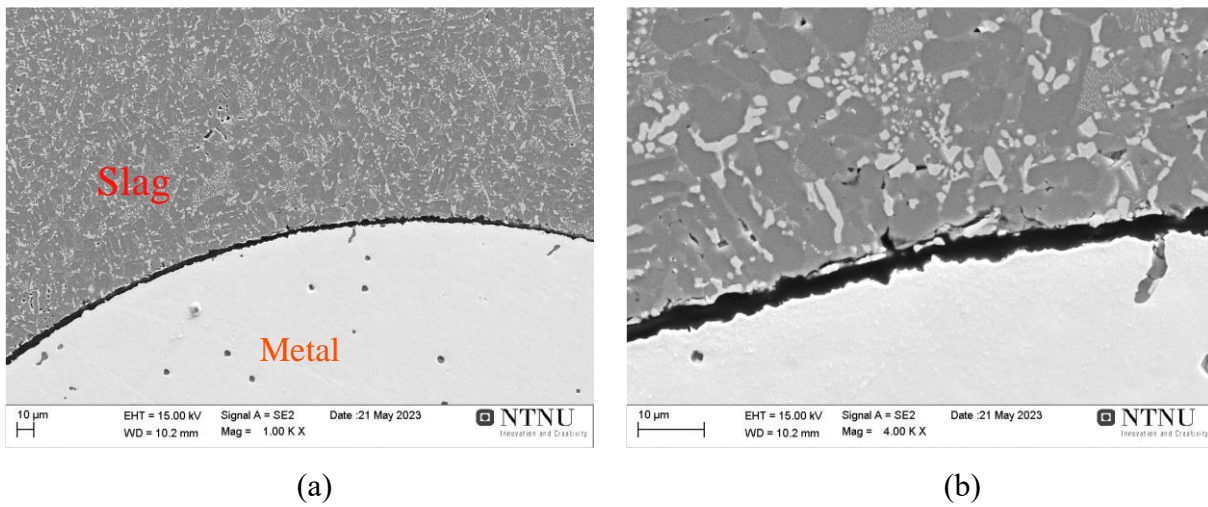


Figure 4-16: The microstructure of 14-0.8 sample.

The same microstructure for the slag was found throughout the sample and EDS mapping of an area is shown in Figure 4-17. One bright phase containing Mn and Fe is seen, as well as two darker phases where both seem to contain Ca, together with Al in the darkest phase.

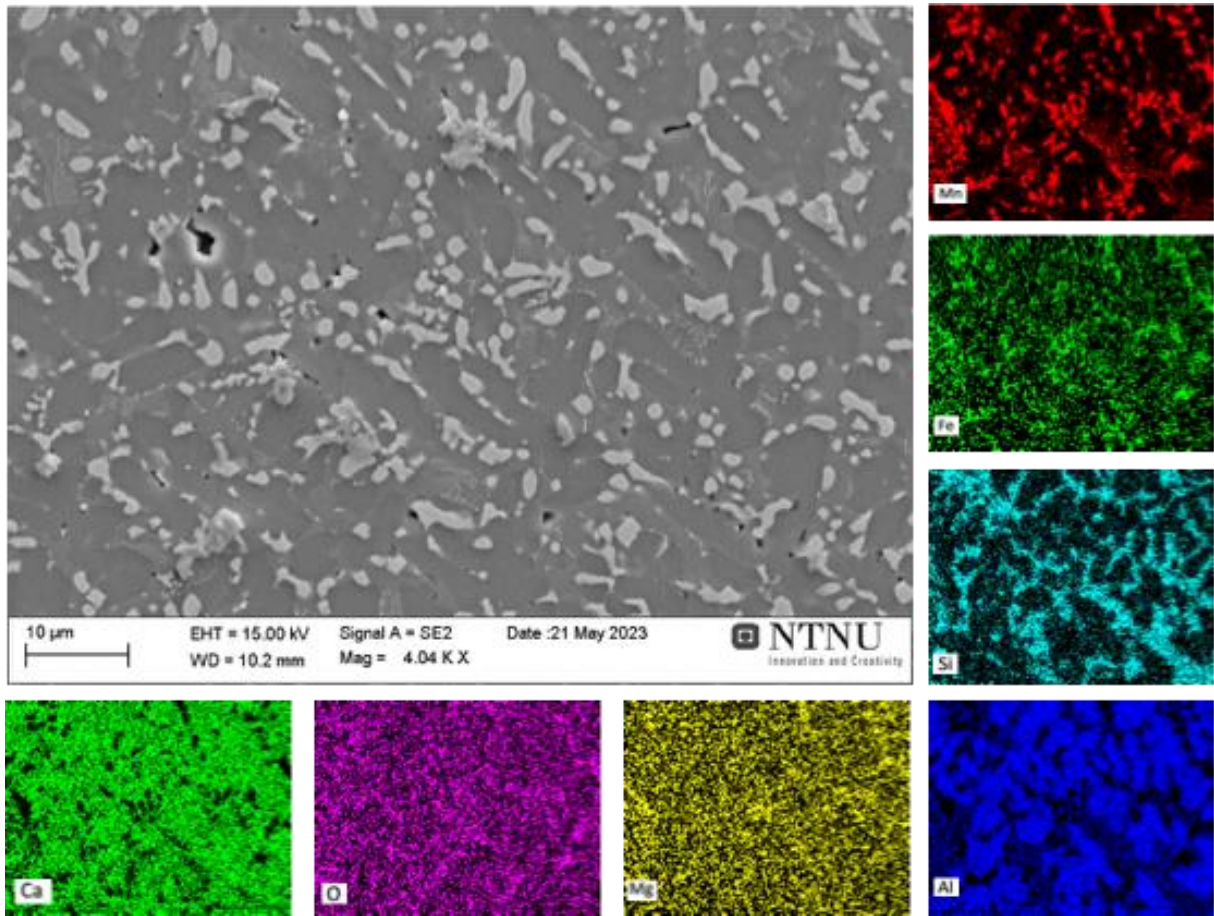
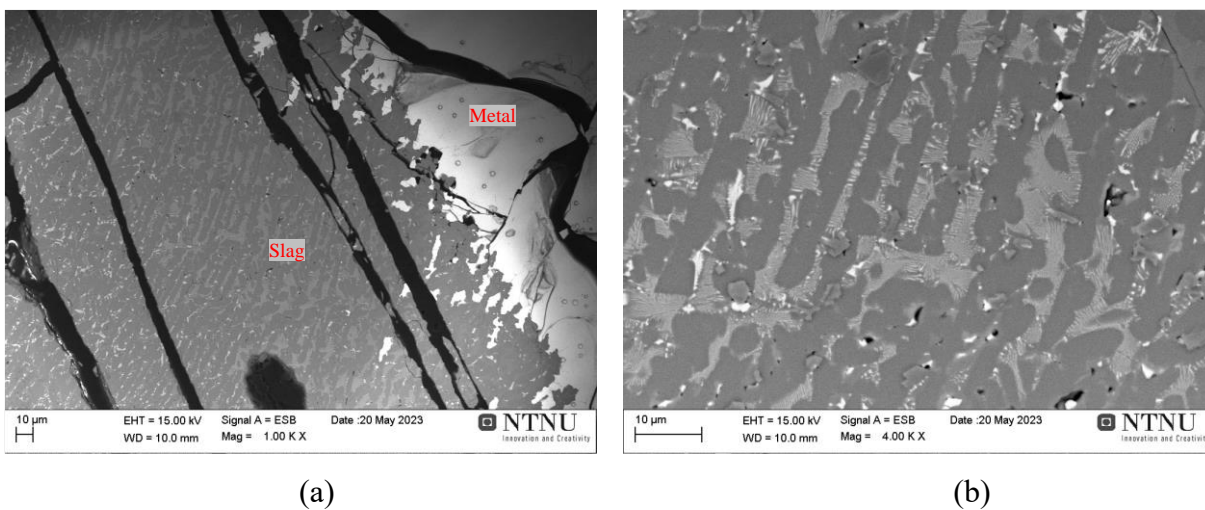


Figure 4-17: Elemental EDS mapping of 14-0.8.

For the 15-1.0 sample, the metal and slag phase can be observed in Figure 4-18 (a). It is observed that smaller metal phases are forming close to the large metal phase. In the slag, three phases are observed.



(a)

(b)

Figure 4-18: The microstructure of 15-1.0 sample.

EDS mapping, Figure 4-19, of sample 15-1.0 shows that the bright phase contains Mn and Fe. Oxygen, Ca and Al are absent in the metal phase. K is observed in the metal phase. The slag contains two main phases, dependent on the Ca and Al content. A fourth phase of Mg and O is observed close to the metal phase.

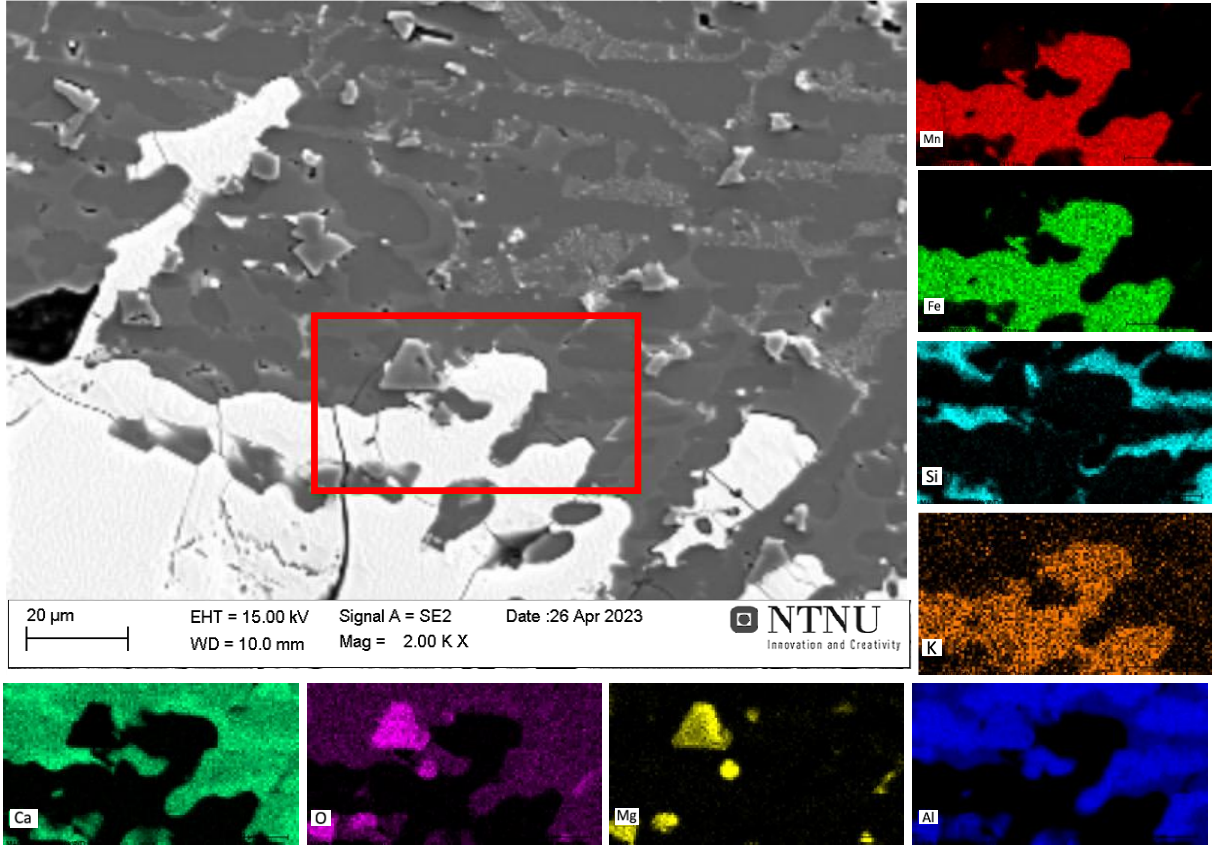


Figure 4-19: Elemental EDS mapping of sample 15-1.0.

Figure 4-20 (a) gives an overview of the slag phase of the 15-0.8 sample where the darkest phase was observed as irregular shapes with flat surfaces, or crystals. In figure (b) the brighter area includes two phases.

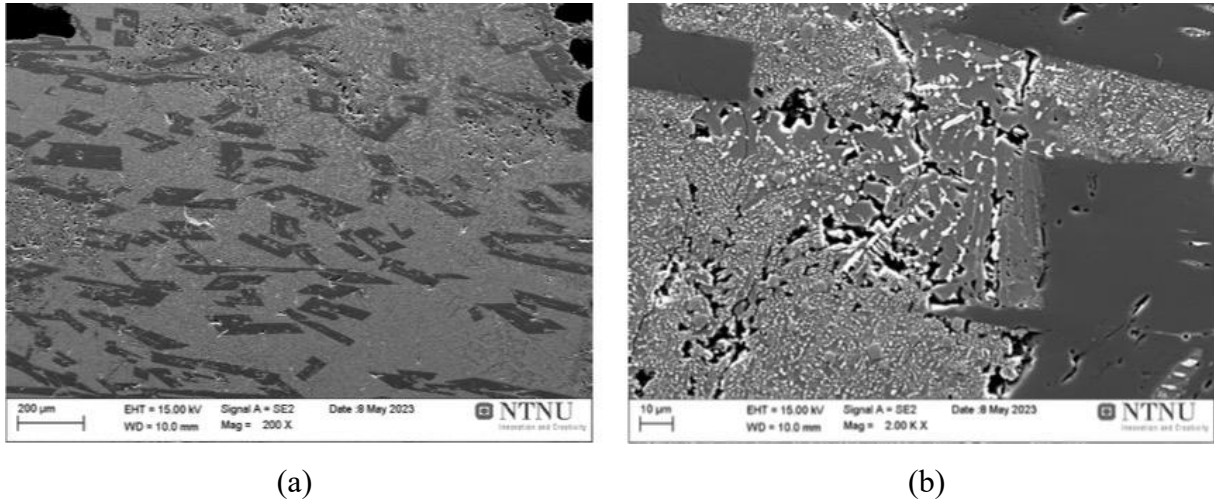


Figure 4-20: The microstructure of the 15-0.8 sample.

Elemental EDS mapping of sample 15-0.8 is shown in Figure 4-21 where the darkest phase is shown to include Al and O. The brightest phase includes Mn and Fe. The third phase includes Ca, Al, O, and Si. A phase of Mg and O is observed in the bottom right corner.

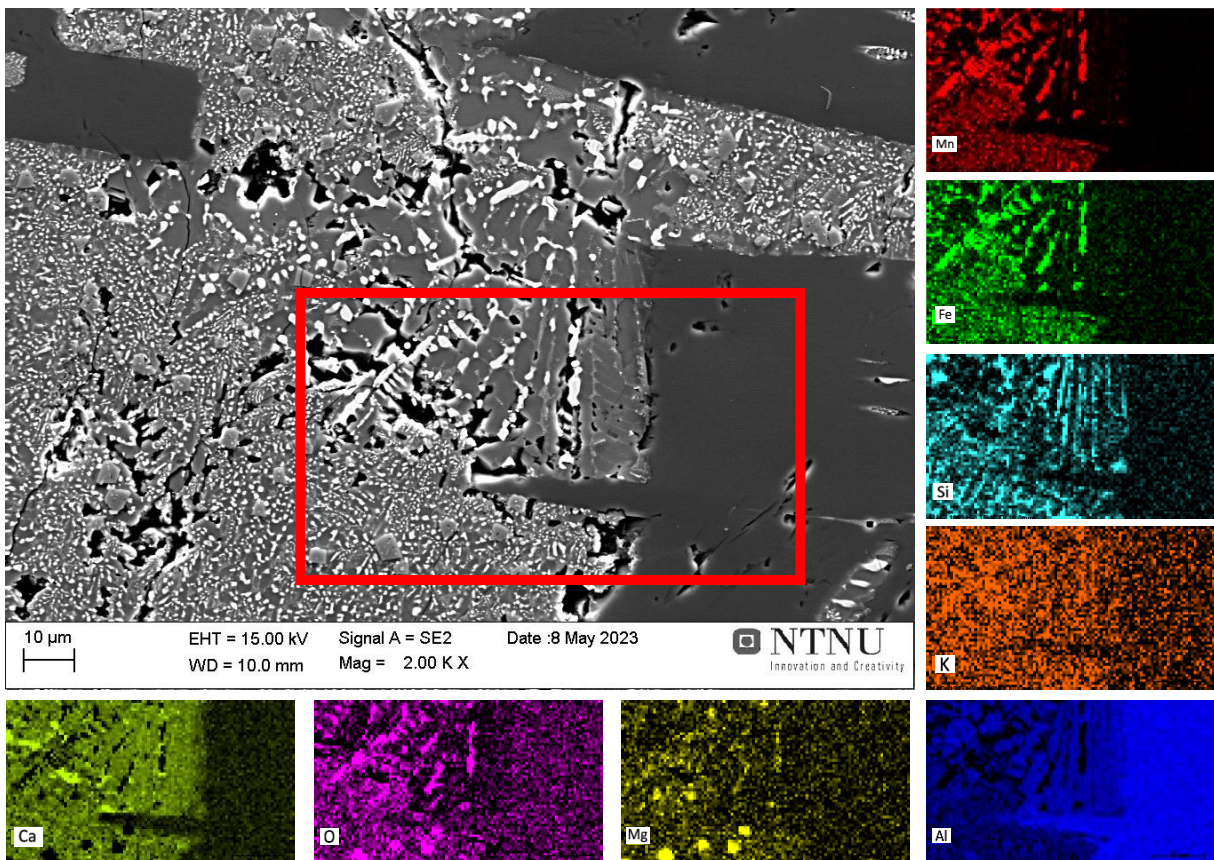


Figure 4-21: Elemental EDS mapping of 15-0.8.

Figure 4-22 shows the EDS mapping for the slag of the 15-0.5h sample. Three phases were observed. Mg and O were found in squared shapes and Fe and Mn were also included here. Mn, Fe, and Si were observed as a second phase, and lastly, Al and Ca are observed in a phase with O.

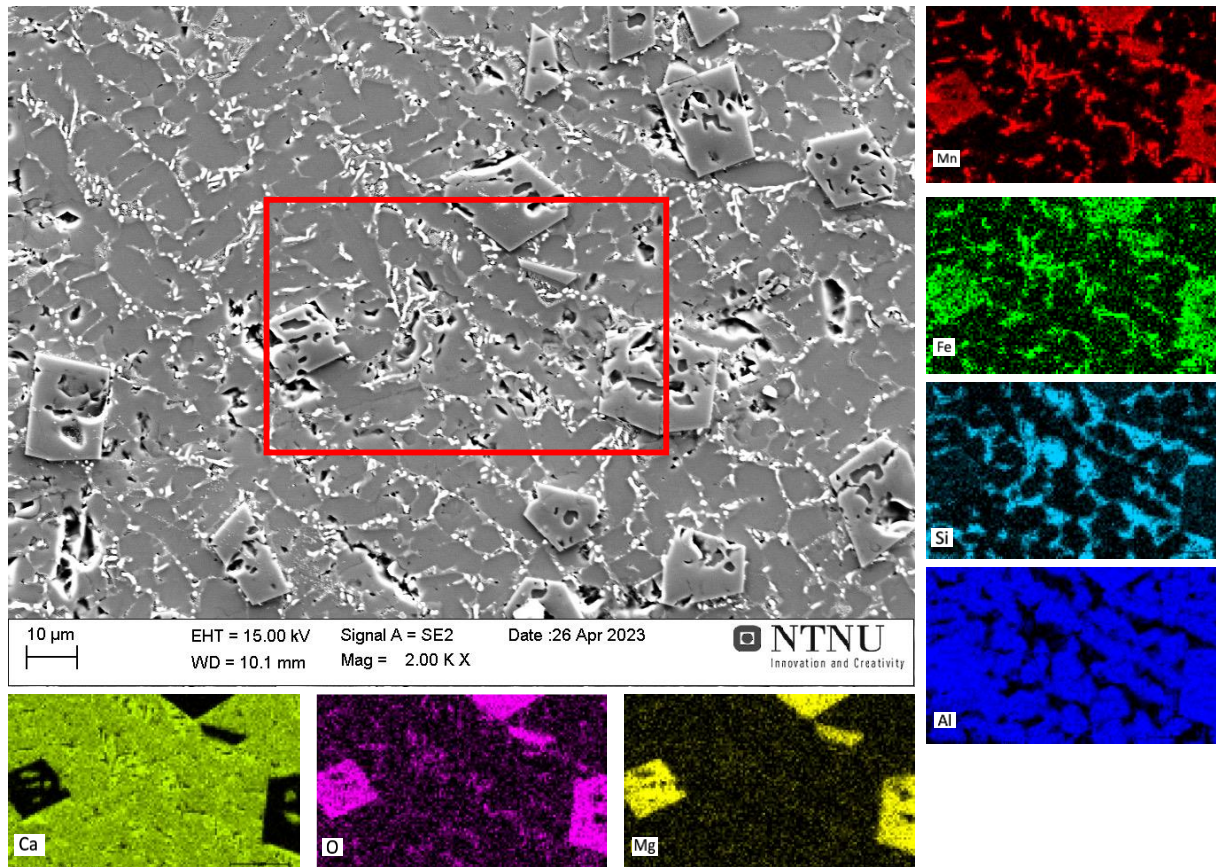


Figure 4-22: Elemental EDS mapping of 15-0.5h sample.

Figure 4-23 shows the metal and slag phase microstructure for the 15-1.5 sample. The slag phase contains three visible phases.

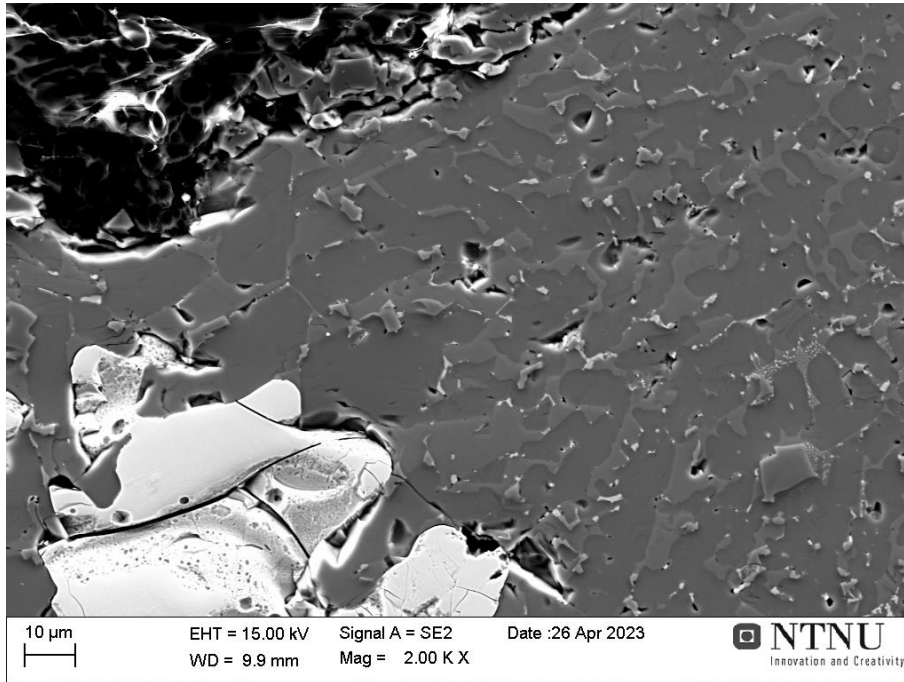


Figure 4-23: The microstructure of the 115-1.5h sample.

Figure 4-24 shows the EDS mapping of the slag and metal phase for the 15-1.5h sample. Mn, Fe, and some O and Si are observed in the metal phase. The slag contains three phases where Ca, Al, and O are observed in the darkest phase, as well as in the two other phases. The brighter slag phase also contains Si. The third phase mainly contains Mg and O as smaller particles.

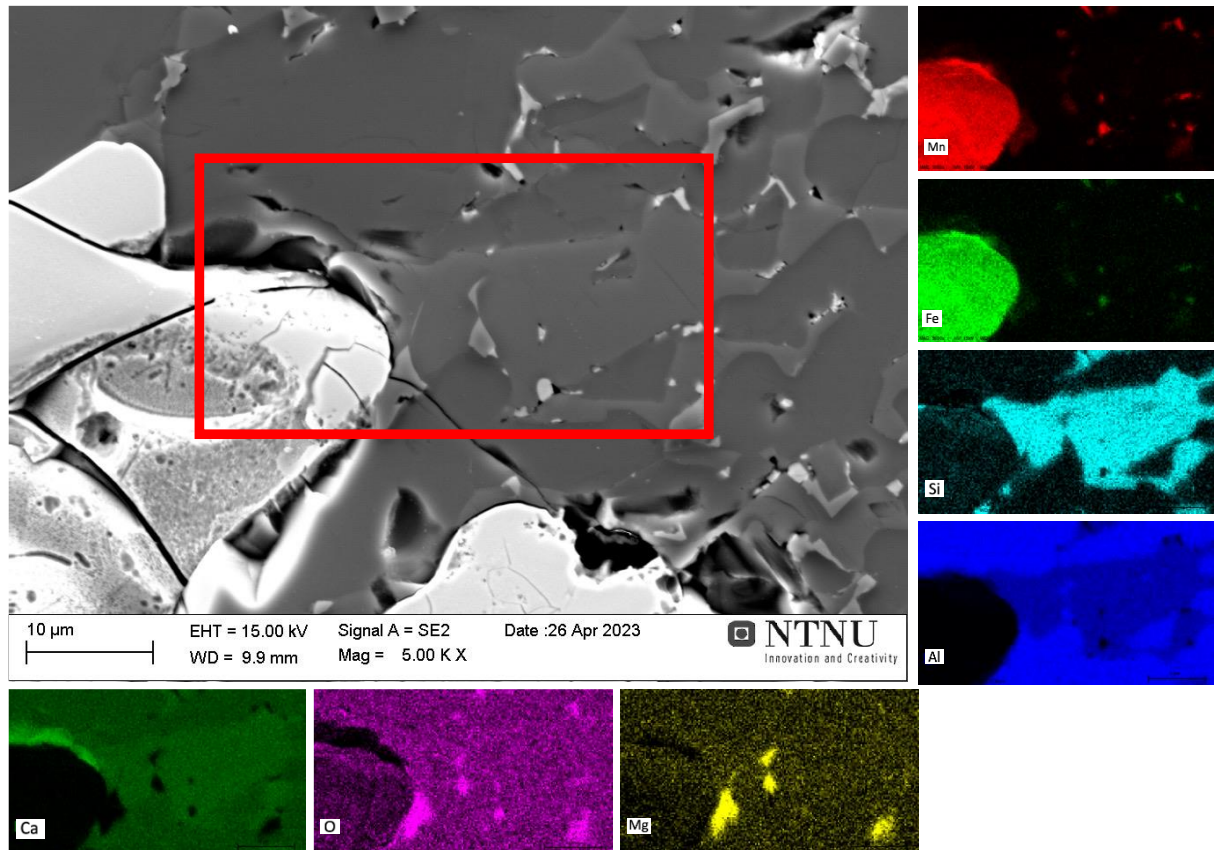


Figure 4-24: EDS mapping of 15-1.5h

4.2.2 Produced metals compositions

The metal compositions were found by EDS point and area analysis performed in metal areas for the samples. 3-4 large areas of the metal phase were analyzed for each sample. This data was the normalized and an average composition for the metal phase of each sample were calculated, and presented in Table 4-4. For sample 13-1.0, Ca, Al, Si, and O measurements are at the highest, and the Mn-Fe content was 79.48%. For the other samples, the metal phase's Mn-Fe content varied from 97.44 to 99.09%

Table 4-4: The measured compositions of metals in the samples.

Element	13-1.0	13-0.8	14-1.0	14-0.8	15-1.0	15-0.8	15-0.5h	15-1.5h
Mn	61.67	69.80	65.44	64.67	67.76	62.90	68.13	68.12
Fe	17.81	27.64	33.61	33.86	30.97	36.01	30.96	30.28
Mn-Fe	<u>79.48</u>	<u>97.44</u>	<u>99.05</u>	<u>98.53</u>	<u>98.73</u>	<u>98.91</u>	<u>99.09</u>	<u>98.4</u>
O	3.34	1.83	0.70	0.90	0.42	0.15	0.05	0.19
Si	4.60	0.60	0.83	0.27	0.52	0.89	0.72	1.35
Mg	0.04	0.02	0.03	0.07	0.13	0.01	0.00	0.01
Ca	6.08	0.03	0.01	0.10	0.18	0.00	0.12	0.02
Al	16.45	0.07	0.02	0.12	0.05	0.03	0.01	0.02
K	0.02	0.02	0.00	0.00	0.00	0.01	0.00	0.01

4.2.3 Slag composition and phases

Like the metals compositions, the overall slags composition were found by EDS point and large area analysis performed in slag areas for the samples. The average was made based on 3-4 area scans of the slag phase and is presented in Table 4-5.

Table 4-5: The measured compositions of oxides in the samples.

Oxide	13-1.0	13-0.8	14-1.0	14-0.8	15-1.0	15-0.8	15-0.5h	15-1.5h
Al ₂ O ₃	48,86	35,44	29,20	42,22	34,16	44,03	35,98	44,76
CaO	24,12	23,13	23,74	36,93	30,16	21,34	29,35	24,45
SiO ₂	3,02	0,80	1,44	4,22	6,35	3,12	3,44	3,09
MnO	15,36	33,11	22,31	31,41	8,82	11,48	6,53	7,77
MgO	1,10	0,25	1,01	0,75	0,35	0,62	0,32	0,34
K ₂ O	0,50	0,64	0,47	0,39	0,18	0,54	0,37	0,31
P	1,23	0,02	0,54	0,03	0,03	1,07	0,54	0,98

Metallic Fe was also found in the overall area scan of the slag phase and the results are presented in Table 4-6.

Table 4-6: Metallic Fe was also present in the slag.

	1310	1308	1410	1408	1510	1508	15-0.5h	15-1.5h
Fe	6.84	7.64	7.26	7.27	7.64	6.31	0.59	5.95

4.2.4 Phase analysis of produced slags

Results from XRD phase analysis are presented in Figure 4-25 for the slag phases of the samples after aluminothermic reduction. Similar phases were found in all the samples.

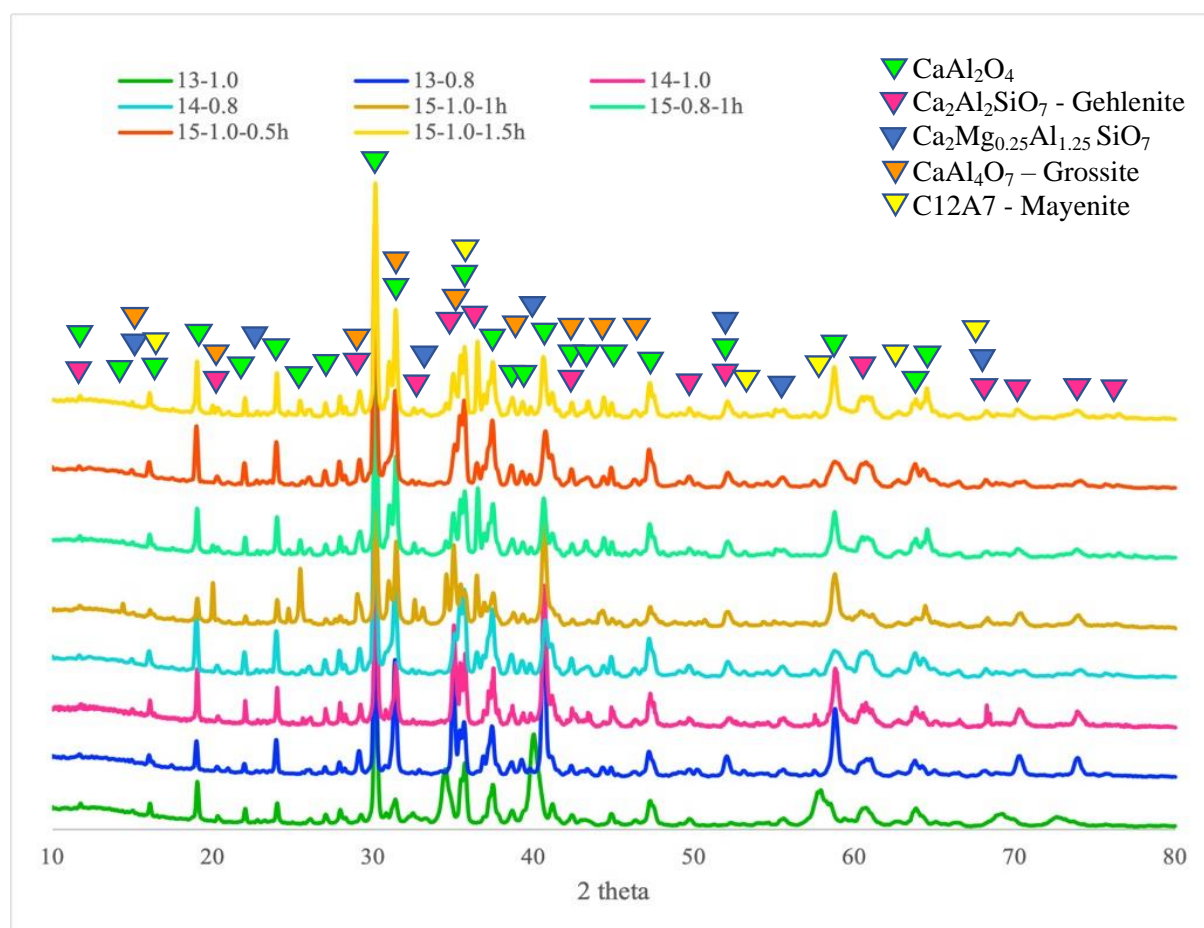


Figure 4-25: XRD phase analysis of samples and the identified phases after aluminothermic smelting reduction.

4.2.5 Mass loss and visual observations

The color of the produced slags was green for all samples after the aluminothermic smelting reduction, and the intensity of the color was somewhat different for the different processing times and temperatures. In Figure 4-26, samples 13-1.0 and 15-1.0 are compared, where the first, (a), was observed to have a stronger and darker green color than the second one, (b), where some parts of the slag had a light green color and white color. As seen in (a), the metal phase formed several droplets throughout the slag, while the 15-1.0 sample had one large metal droplet. All samples can be seen in Appendix 3.



(a)

(b)

Figure 4-26: shows two samples, (a) and (b), after processing. Sample (a) is 13-1.0 and (b) is 15-1.0-1h

The mass loss for the samples varied between 1.21-5.15wt% as displayed in Table 4-7.

Table 4-7: The mass loss of samples after aluminothermic smelting reduction.

Sample	Mass loss [g]	Mass loss [%]
13-1.0	0.28	1.92
13-0.8	0.13	1.21
14-1.0	0.58	3.51
14-0.8	0.55	5.15
15-1.0	0.58	3.93
15-0.8	0.33	1.44
15-0.5h	0.42	2.26
15-1.5h	0.59	3.40

5. Discussion

As presented before 4 smelting and 8 smelting-reduction tests were executed. The effect of chemical composition on smelting and smelting-reduction, as well as temperature and holding time for aluminothermic smelting reduction are discussed as follows.

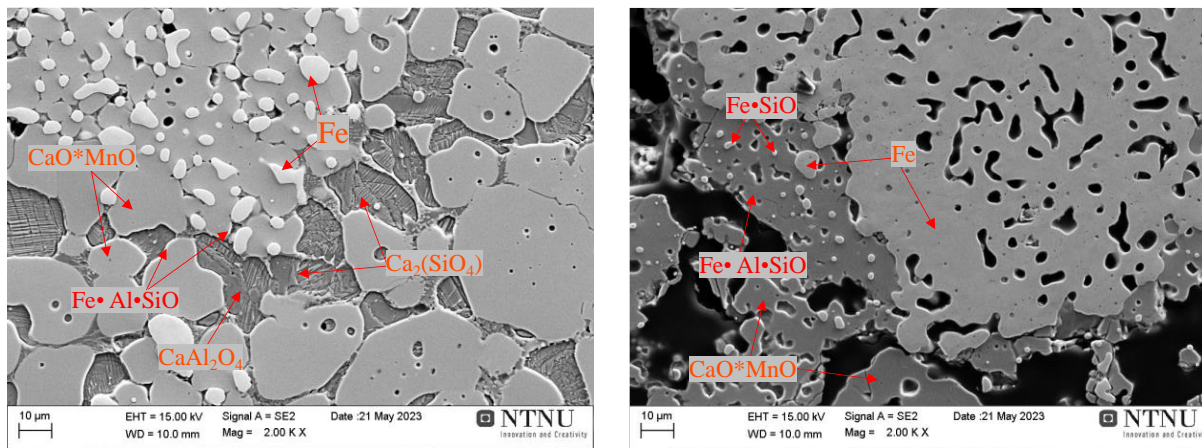
5.1 Effect of temperature on the flux-smelting on pre-reduced ore

For both the 1 molar relationship and 0.8 molar relationships for $\text{CaO}/\text{Al}_2\text{O}_3$, endothermic behavior was observed during heating in DSC. The drop at 400°C could be in relation to mass loss observed from the TG-analysis, where a drop in the mass is observed at this temperature. The mass loss in this area presumably is loss of volatiles and/or structural moisture. It is possible to have small amount of $\text{Ca}(\text{OH})_2$ due to the exposure of CaO with air and interaction with the room humidity, and the decomposition of $\text{Ca}(\text{OH})_2$ to CaO and $\text{H}_2\text{O}(\text{g})$ occurs at these temperature ranges. Between $1400\text{-}1500^\circ\text{C}$ a further reduction in the power flow was observed, but no clear indication of melting can be analyzed from this.

From the phase analysis, similar phases were found for both samples smelted in the tube furnace. A phase CaAl_2O_4 was also observed for the 1 molar $\text{CaO}/\text{Al}_2\text{O}_3$. The mass fraction of Al_2O_3 in the pre-reduced Mn ore and Lime are 1.01wt% and 0.16wt%, respectively, and the CaAl_2O_4 phase was detected with 20.01% Al_2O_3 . The crucibles used in the resistance tube furnace were Al_2O_3 -crucibles and some diffusion of Al_2O_3 might have occurred into the smelted Mn-ore and Lime mixture, giving some Al_2O_3 into the slag. When looking at the sample in Figure 4-2 the sample is clearly sintered to the crucible, and the green residue suggests some reaction with Al_2O_3 and MnO could have occurred.

As seen in Figure 2-10, the MnO - CaO phase diagram shows MnO and CaO as completely miscible in both solid-state and liquid-state. For the 1 molar $\text{CaO}/\text{Al}_2\text{O}_3$ sample physical observations and phase analysis suggests that the sample was smelted. The 0.8 molar ratio $\text{CaO}/\text{Al}_2\text{O}_3$ sample showed similar phases from XRD analysis, but physical observations of the sample suggested the sample components were sintered together, and not smelted. This suggests solid state diffusion and surface melting/fusion occurred.

The difference in the smelting behavior for samples 1 and 0.8 was also observed in the microstructural analysis. As expected from the phase diagram in Figure 2-10, MnO-CaO solid solutions was found in both samples and this indicates that the pre-reduced fine ore particles interacted with the fine CaO particles and a dominant CaO-MnO solid solution has been formed as the corresponding phase diagram (Figure 2-10) indicate. The other observed phases in the XRD (Figure 4-5) and microstructure of these slags (Figure 5-1), such as Ca_2SiO_4 and FeAlSiO , are also predicted regarding the phase diagrams of $\text{CaO-Al}_2\text{O}_3\text{-SiO}_2$ and $\text{CaO-MnO-Al}_2\text{O}_3$.



(a)

(b)

Figure 5-1: The smelted Ore-lime samples is presented with phases found from XRD and EDS mapping, where (a) is the 1 molar $\text{CaO}/\text{Al}_2\text{O}_3$ and (b) is the 0.8 molar $\text{CaO}/\text{Al}_2\text{O}_3$.

5.2 Metal yield and mass loss in aluminothermic reduction trials

All the samples undergoing aluminothermic smelting reduction obtained a molten state and then solidified, resulting in a slag and a metal phase in each sample. This was also achieved in samples at 1300°C , although some overshooting of temperature in the furnace during heating caused higher temperatures in the sample, probably initiating the aluminothermic reduction.

The composition of the produced metals is shown in Figure 5-2 where the samples at 1300°C has a lower content of Mn and Fe than the samples processed at higher temperatures.

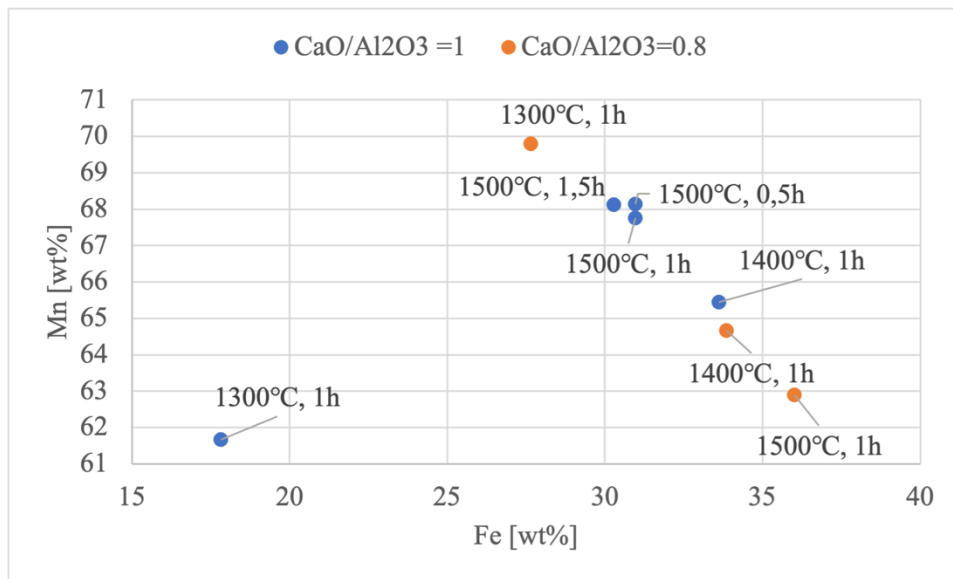


Figure 5-2: The Mn and Fe content in the metal phase from Table 4-4 is showed in the plot.

The samples with the 1 CaO/Al₂O₃ were found to have a similar Mn-Fe ration at 1500°C. For the 0.8 CaO/Al₂O₃, the increase in temperature led to an increase of Fe in the metal phase.

5.3 Effect of the temperature on aluminothermic reduction

As mentioned, all the samples underwent an aluminothermic smelting reduction. The reduction probably occurred to a smaller extent at 1300°C since a larger amount of oxygen was found in the phase analysis of these samples. This was also visible as the slag from the lower-temperature samples was observed to have a clearer and stronger green color than the samples at higher temperatures.

The temperature had a clear effect on the yield of metal from the slag, as seen in Figure 5-3, where the wt% of MnO left in the slag increases for the 1 molar and 0.8 CaO/Al₂O₃ samples as the processing temperature is raised.

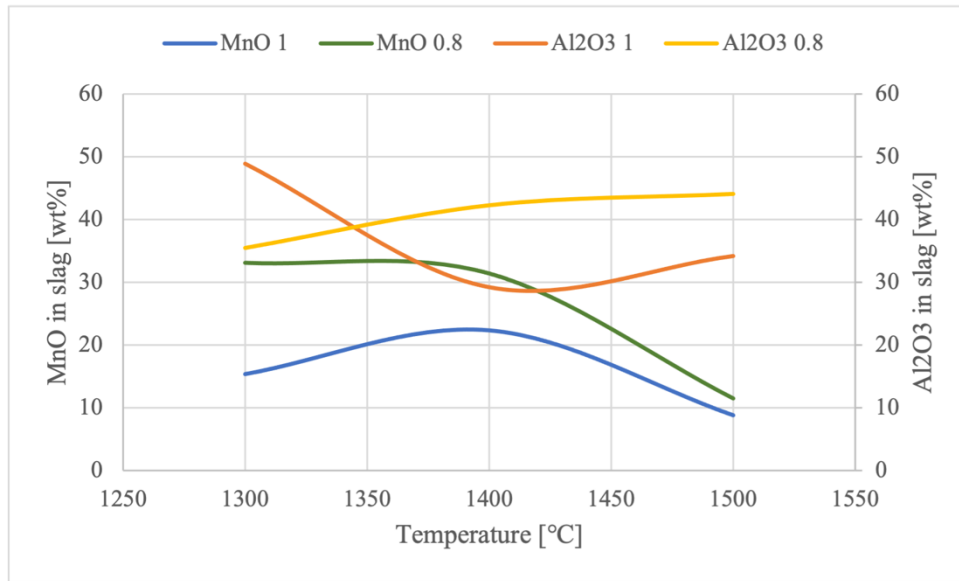


Figure 5-3: The MnO and Al₂O₃ present in the slag presented in Table 4-5 is shown as a function of temperature.

The observations of the change in green color also align with the findings from the EDS area scans of the slags.

5.4 Effect of processing time

Figure 5-4 shows that the metal phase assembled into one big metal droplet at this temperature in the bottom of the crucible, making it easily separatable from the slag. The color observed in the slag for (c), held at 1.5h at 1500°C, was slightly lighter than (a) and (b).

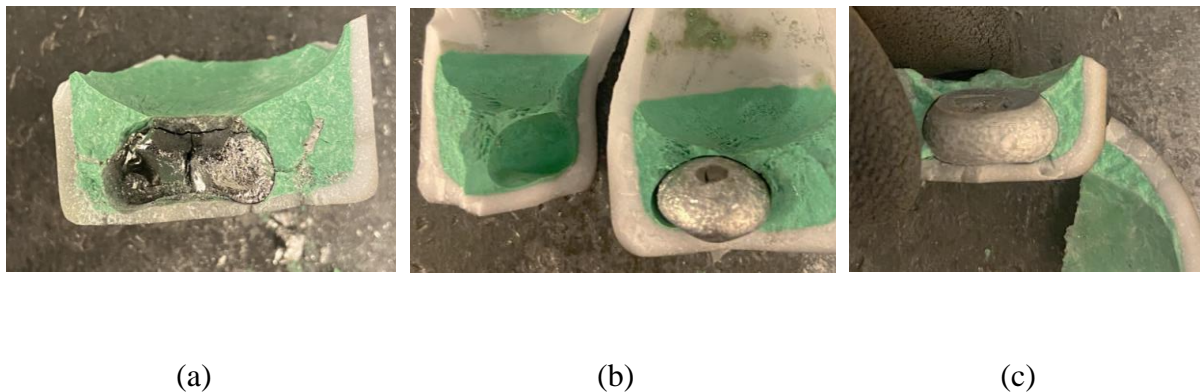


Figure 5-4: Pictures of the samples reduced at 1500°C the 1 molar CaO/Al₂O₃, where (a) had a holding time of 0.5h, (b) a holding time of 1h, and (c) a holding time of 1.5h.

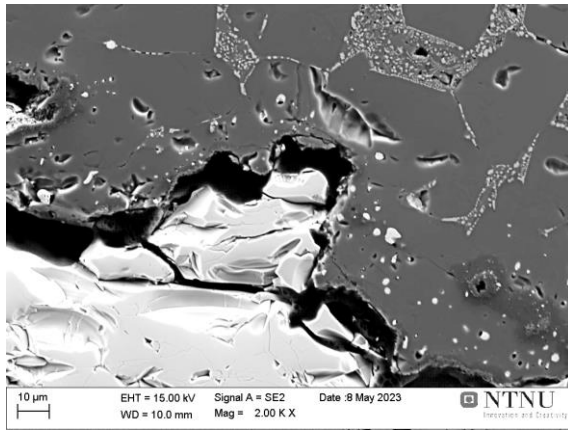
When looking at the composition of the slag measured by EDS area scan, the sample processed for 1.5h contained the least MnO, as seen in Figure 5-3. As the color of the slag and the EDS area scan suggests, the yield of Mn is not 100% at these conditions. Obviously, the rate of the aluminothermic reduction is quite high and the process time did not affect the proceed of reaction significantly.

5.5 Characteristics of the produced slags

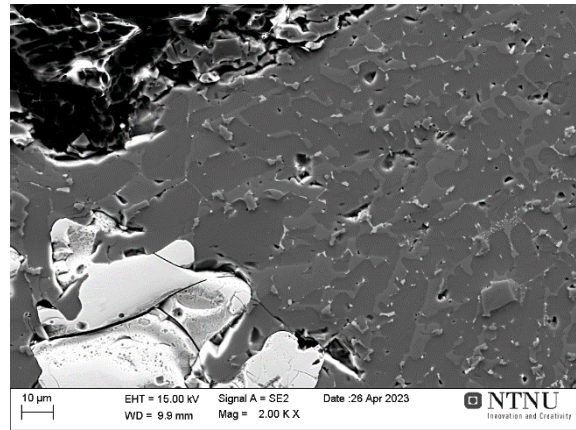
No free particles of Al_2O_3 or CaO were observed in the microstructural analysis of the slag, indicating that the mixing of these compounds was complete during the aluminothermic reaction. This suggests that the slag composition is overall homogeneous, confirming that all the material became fully molten due to the temperature rise as significant heat is generated during the aluminothermic reduction. No unreacted Al was found in the phase analysis of the slag, even though some MnO was still present in the slag phase. A little unreacted Al in the system has been dissolved in the produced Mn-Fe alloys as presented in Table 4-4.

Mayenite, C12A7, was found in the phase analysis by XRD, which corresponds to the findings of [17] [20]. This is seen as favorable since the C12A7 phase is the most leachable $\text{CaO-Al}_2\text{O}_3$ phase and is interesting for further use of the slag in alumina recovery by leaching [17].

Small droplets and areas of metallic phases were found in the samples at lower processing temperatures. As seen in Figure 5-5 (a), light particles are clustered together in the slag around the metal phase. For (b), at a higher processing temperature, these particles are not seen to the same extent, giving a higher metal yield agreeing with the findings from the EDS area scans.



(a)



(b)

Figure 5-5: The microstructure of the slag phase close to the metal phase is presented for 1 molar and $\text{CaO}/\text{Al}_2\text{O}_3$ samples at temperature 1300°C (a) and 1500°C (b).

The existence of the tiny metal particles in the slag matrix may be due to the not enough time for their settling or the viscosity of the slag. Obviously, lower viscosity will enhance the metal droplets movement to the crucible bottom.

6. Conclusions

- In this master thesis, experimental work was done to study the smelting and smelting reduction of a pre-reduced Mn ore by lime and Al metal, and the following conclusion can be presented.
- Smelting occurs for more CaO addition and for higher targeted CaO/Al₂O₃ ratio (equal to 1) at 1500°C.
- Sintering occurred for 0.8 molar CaO/Al₂O₃ sample at 1500°C.
- Metallic Mn was yielded for all samples undergoing aluminothermic smelting reduction from 1300-1500°C.
- The extent of reaction was lower for aluminothermic reduction occurring at 1300°C.
- The processing time was found to have some effect on the extent of reduction, but the increased processing temperature had the biggest effect on MnO left in the slag.
- The leachable mayenite (C12A7) phase was found in the produced slags as the main Al₂O₃-containing compound, and it is proper for further alumina recovery from the slags.

7. Further work

- DTA to obtain more accurate information about smelting behavior and smelting points for pre-reduced Mn-ore and the effect of lime addition.
- Further investigation into effect of lime-flux composition on reaction.
- Further investigation into temperature effect on metal yield for the reaction.

Bibliografi

- [1] S. E. Olsen, M. Tangstad og T. Lindstad, *Production of Manganese Ferroalloys*, 2007, Tapir akademisk forlag.
- [2] J. Safarian, «Duplex Process to Produce Ferromanganese and Direct Reduced Iron by Natural Gas,» *ACS Sustainable Chem. Eng.*, 2021.
- [3] J. Safarian, «A Sustainable Process to Produce Manganese and Its Alloys through Hydrogen and Aluminothermic Reduction,» *Process*, vol. 10, nr. 27, 2022.
- [4] European Commission, «Study on the Critical Raw Materials for the EU 2023 – Final Report,» 2023.
- [5] A. H. Sully, *Manganese*, New Yorke: Academic Press, 1955.
- [6] A. H. Reidies, «Manganese Compounds,» i *Ullmann's Encyclopedia of Chemical Technology 2007*, Wiley-VCH.
- [7] B. Sørensen, S. Gaal, E. Ringdalen, M. Tangstand, R. Kononoc og O. Ostorovski, «Phase compositions of manganese ores and their change in the process of calcination,» *International Journal of Mineral Processing*, 2010.
- [8] «U.S. Geological Survey,» *Mineral commodity summaries*, 2022.

- [9] A. Cheraghi, H. Yoozbashizadeh og J. Safarian, «Gaseous Reduction of Manganese Ores: A Review and Theoretical Insight.,» *Mineral Processing and Extractive Metallurgy Review*, pp. 198-215, 2020.
- [10] E. Nyhus, «An investigation in characterization and pre-reduction behavior of manganese ore in hydrogen,» Norwegian University of Science and Technology Department of Materials Science and Engineering, 2022.
- [11] O. Dávila, J. Torres og A. Valdes, «Effect of Mg Concentration on the Aluminothermic Reduction of Mn₂O₃ Particles Obtained from Cathodes of Discharged Alkaline Batteries: Mathematical Modeling and Experimental Results.,» *Materials*, nr. 9, p. 49, 2019.
- [12] R. Kavitha og J. McDermid, «On the in-situ aluminothermic reduction of manganese oxides in continuous galvanizing baths.,» *Surface and Coatings Technology*, nr. 212, pp. 152-158, 2012.
- [13] S. Jixing, G. Tao, D. Wen, M. Yiming, F. Xiang og W. Hao, «Study on Thermal Chemical Reaction of Al/MnO₂ Thermite». *IOP Conference Series: Earth and Environmental Science*.
- [14] B. Sarangi, A. Sarangi og H. S. Ray, «Kinetics of Aluminothermic Reduction of MnO₂ and Fe₂O₃: A Thermoanalytical Investigation,» pp. 1135-1141, 1996.
- [15] B. Bhoi, B. Murthy, P. Datta, Rajeev og A. Jouhari, «Studies on Aluminothermic Reduction of Manganese ore for Ferro- Manganese Making.,» *Ferro Alloy Industries in the Liberalised Economy*, p. 66–70. , 1997.

- [16] A. Kudyba, S. Akhtar, I. Johansen og J. Sarfarian, «Aluminothermic Reduction of Manganese Oxide from Selected MnO-Containing Slags.,» *Materials*, nr. 14, p. 356, 2021.
- [17] A. Kudyba og J. Safarian, «Manganese and Aluminium Recovery from Ferromanganese Slag and Al White Dross by a High Temperature Smelting-Reduction Process.,» *Materials*, nr. 15, p. 2022, 2022.
- [18] R. Gee og T. Rosenquist, «The Vvapour pressure of liquid manganese and activities in liquid MnSi and carbon-saturated Mn-Si alloys,» *Scandinavian Journal of Metallurgy*, pp. 57-62, 1974.
- [19] R. Hultgren, P. Desai, D. Hawkins, M. Gleiser og K. Kelley, «Selected Values of the Thermodynamic Properties og Binary Alloys,» *American Society for Metal*, 1973.
- [20] F. Azof, K. Tang, J. You og J. Safarian, «Synthesis and Characterization of 12CaO·7Al₂O₃ Slags: The Effects of Impurities and Atmospheres on the Phase Relations.,» *Metall Mater Trans B*, p. 2689–2710, 2020.
- [21] I. Hallsteinsen, *Lecture notes from TMT4301 - Materials Characterization*, NTNU, 2022.
- [22] H. B., «Assessment of the CaO–Al₂O₃ system,» *Journal of the American Ceramic Society*, nr. Vol. 73, pp. 15-23, 1990.
- [23] S. E.S., R. G.A. og W. F.E., *American Journal of Sciense*, Vol. %1 av %2vol- 28, pp. 293-333, 1909.

- [24] G. W. H. Höhne, W. F. Hemminger og H. J. Flammersheim, *Differential Scanning Calorimetry*, Springer-Verlag: Berlin Heidelberg New York , 2003, pp. 1-2, 10-12, 17-20, 115-117.
- [25] R. C. Mackenzie, «Nomenclature in thermal analysis,» *Thermochim Acta*, pp. 1-6, 1979.
- [26] M. Ladd og R. Palmer, *Structure Determination by X-ray Crystallography - Analysis by X-rays and Neutrons*, Springer, 1977.
- [27] J. Hjelen, *Scanning electronmikroskopi (compendium)*, 1986.
- [28] J. I. e. Goldstein, *Scanning Electron Microscopy and X-ray Microanalysis*, 2018.
- [29] H. E. Barner og C. L. Mantell, «Kinetics of hydrogen reduction of manganese dioxide,» *Industrial & Engineering Chemistry Process Design and Development*, pp. 285-294, 1968.
- [30] N. R. W. , W. J. H. og M. A. J. , «Trans. Br. Ceram. Soc.,» nr. vol. 64, pp. 409-418, 1965.

Appendix

Appendix 1

Calculation of sample masses

Oxid	[wt%]	Oxid	[wt%]
CaO	<u>6,90</u>	Na ₂ O	<u>0,75</u>
MgO	<u>2,83</u>	K ₂ O	<u>0,28</u>
SiO ₂	<u>4,99</u>	P ₂ O ₅	<u>0,84</u>
Al ₂ O ₃	<u>1,01</u>	SO ₃	<u>0,16</u>
Fe	<u>13,65</u>	SrO	<u>0,22</u>
MnO	<u>67,83</u>	BaO	<u>0,18</u>
Cr ₂ O ₃	<u>0,02</u>	Cl	<u>0,10</u>
TiO ₃	<u>0,02</u>	CeO ₂	<u>0,21</u>

Composition 1:

Theoretical yield of Mn from MnO based on reduction by Al:

$$\frac{wt\%MnO * 2 * molar\ mass(Al)}{3 * molar\ mass(MnO)} = Al\ added\ to\ mix$$

$$\frac{67.83g * 2 * 26.98mol}{3 * 71mol} = 17.20g$$

Alumina produced:

$$\frac{toAl\ added\ to\ mix * molar\ mass(Al_2O_3)}{2 * molar\ mass(Al)} = Al_2O_3\ produced$$

$$\frac{17.20g * 101.96mol}{2 * 26.98mol} = 32.48g$$

Total alumina in slag

Alumina produced + alumina in pre reduced MnO

$$32.48g + 1.01g = 33.49g$$

CaO in slag

$$CaO \text{ in slag} = Al_2O_3 \text{ in slag}$$

$$33.49g = 33.40g$$

CaO addition needed

$$CaO \text{ in slag} - CaO \text{ in pre reduced MnO}$$

$$33.49g - 6.90g = 26.59g$$

Lime addition based on calculated CaO addition

$$CaO \text{ addition} * CaO \text{ content in lime}$$

$$26.59g * 0.90 = 29.48g$$

Composition 0.8:

Theoretical yield of Mn from MnO based on reduction by Al:

$$\frac{wt\%MnO * 2 * molar\ mass(Al)}{3 * molar\ mass(MnO)} * 80\% = Al \text{ added to mix}$$

$$\frac{67.83 * 2 * 26.98}{3 * 71} * 80\% = 13.76$$

Alumina produced:

$$\frac{\text{toAl added to mix} * \text{molar mass}(Al_2O_3)}{2 * \text{molar mass}(Al)} = Al_2O_3 \text{ produced}$$

$$\frac{13.76g * 101.96mol}{2 * 26.98mol} = 25.99g$$

Total alumina in slag

Alumina produced + alumina in pre reduced MnO

$$25.99g + 1.01g = 26.99g$$

CaO in slag

CaO in slag = Al₂O₃ in slag

$$26.99g = 26.99g$$

CaO addition needed

CaO in slag – CaO in pre reduced MnO

$$26.99g - 6.90g = 20.10g$$

Lime addition based on calculated CaO addition

*CaO addition * CaO content in lime*

$$20.10g * 0.90 = 22.28g$$

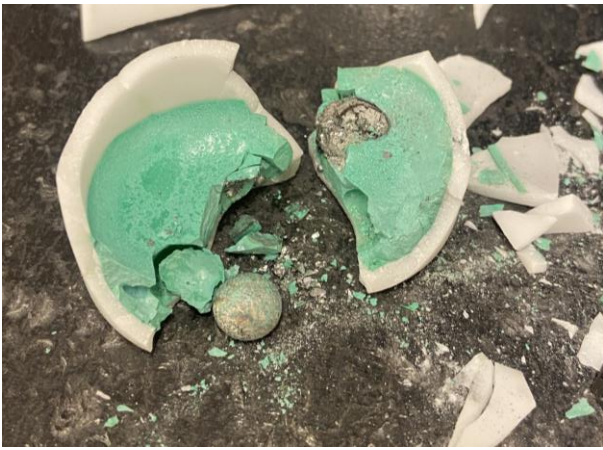

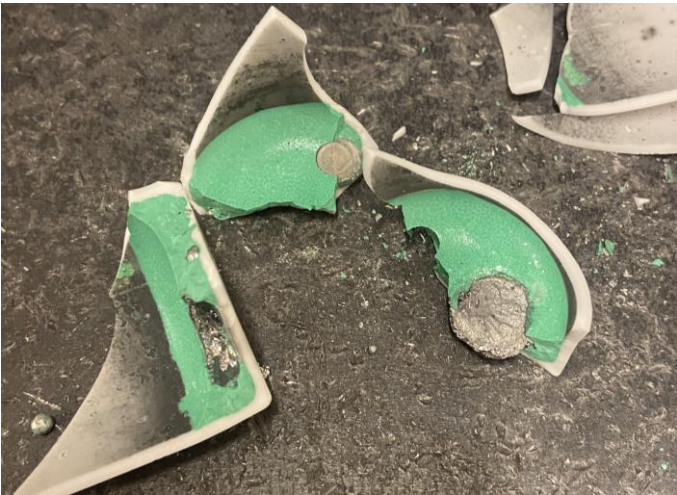

Appendix 2

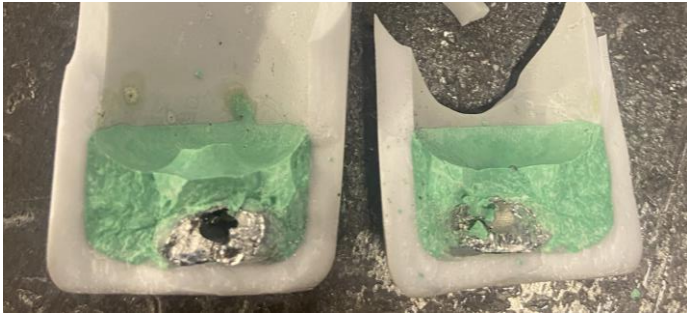
Sample masses

Experiment nr.	Pre-reduced ore [g]	Lime [g]	Aluminium [g]	Total weight of sample [g]	Temperature [°C]	Comment
1	10.70	2.23	1.84	14.77	1300	1
2	8.29	1.67	1.14	11,10	1300	0.8
3	11.74	2.62	2.02	16.38	1400	1.0
4	7.92	1.59	1.09	10.60	1400	0.8
5	10.64	2.37	1.83	14.84	1500	1.0
6	16.72	3.73	2.30	22.75	1500	0.8
7	13.72	2.37	2.36	18.39	1500	1.0 - Holding time 0.5h
8	12.38	2.13	2.76	17.27	1500	1.0 - Holding time 1.5h

Appendix 3

Pictures of samples after aluminothermic reduction

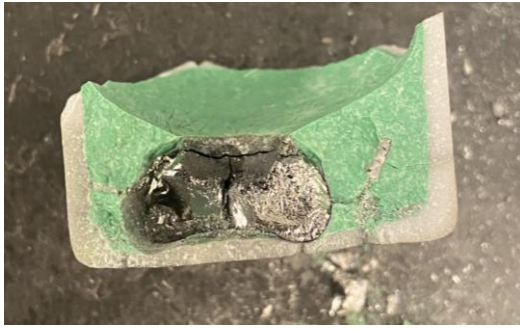
 A photograph showing a broken green sample inside a white container. The sample is fragmented into several pieces, with some showing a dark, porous interior. The container is placed on a dark, textured surface.	 A photograph of a green sample in a white container. The sample is a solid, rounded shape with a central hole. It has a dark, porous appearance. The container is on a dark surface.
13-1.0	13-0.8
 A photograph of a broken green sample in a white container. The sample is fragmented into several pieces, with some showing a dark, porous interior. The container is on a dark, textured surface.	 A photograph of a green sample in a white container. The sample is a solid, rounded shape with a central hole. It has a dark, porous appearance. The container is on a dark surface.
14-1.0	14-0.8



15-1.0



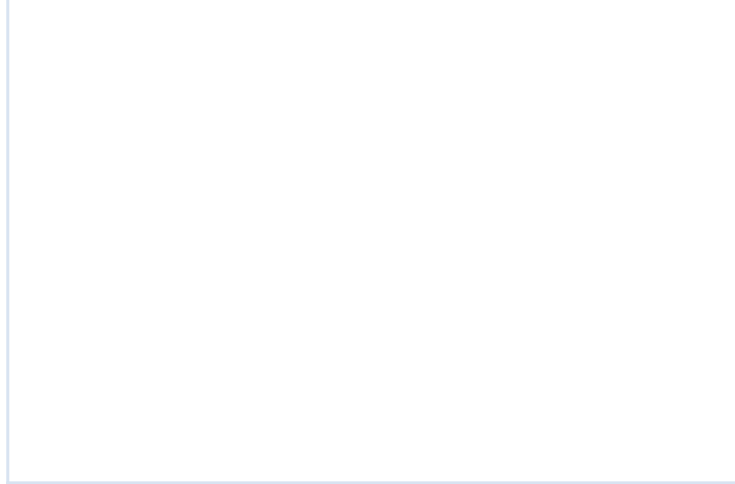
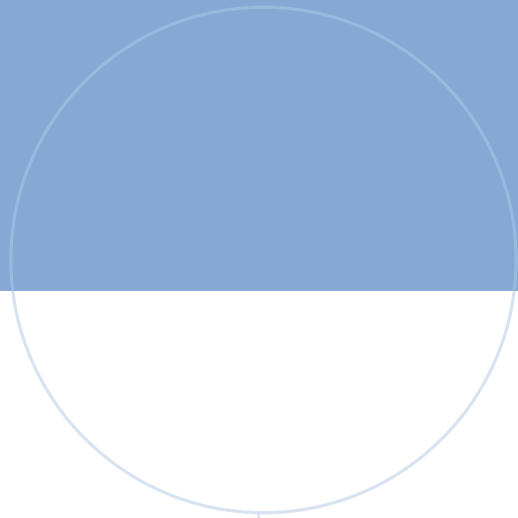
15-0.8



15-0.5h



15-1.5h



 **NTNU**

Norwegian University of
Science and Technology